
Doctoral Dissertations

Student Theses and Dissertations

Summer 2017

Gamma spectroscopy by artificial neural network coupled with MCNP

Huseyin Sahiner

Follow this and additional works at: https://scholarsmine.mst.edu/doctoral_dissertations



Part of the [Nuclear Engineering Commons](#)

Department: Nuclear Engineering and Radiation Science

Recommended Citation

Sahiner, Huseyin, "Gamma spectroscopy by artificial neural network coupled with MCNP" (2017). *Doctoral Dissertations*. 2598.

https://scholarsmine.mst.edu/doctoral_dissertations/2598

This thesis is brought to you by Scholars' Mine, a service of the Missouri S&T Library and Learning Resources. This work is protected by U. S. Copyright Law. Unauthorized use including reproduction for redistribution requires the permission of the copyright holder. For more information, please contact scholarsmine@mst.edu.

GAMMA SPECTROSCOPY BY ARTIFICIAL NEURAL NETWORK COUPLED
WITH MCNP

by

HUSEYIN SAHINER

A DISSERTATION

Presented to the Graduate Faculty of the

MISSOURI UNIVERSITY OF SCIENCE AND TECHNOLOGY

In Partial Fulfillment of the Requirements for the Degree

DOCTOR OF PHILOSOPHY

in

NUCLEAR ENGINEERING

2017

Approved by

Xin Liu, Advisor

Ayodeji B. Alajo

Hyoung K. Lee

Shoaib Usman

Cihan Dagli

Copyright 2017
HUSEYIN SAHINER
All Rights Reserved

ABSTRACT

While neutron activation analysis is widely used in many areas, sensitivity of the analysis depends on how the analysis is conducted. Even though the sensitivity of the techniques carries error, compared to chemical analysis, its range is in parts per million or sometimes billion. Due to this sensitivity, the use of neutron activation analysis becomes important when analyzing bio-samples. Artificial neural network is an attractive technique for complex systems. Although there are neural network applications on spectral analysis, training by simulated data to analyze experimental data has not been made. This study offers an improvement on spectral analysis and optimization on neural network for the purpose. The work considers five elements that are considered as trace elements for bio-samples. However, the system is not limited to five elements. The only limitation of the study comes from data library availability on MCNP. A perceptron network was employed to identify five elements from gamma spectra. In quantitative analysis, better results were obtained when the neural fitting tool in MATLAB was used. As a training function, Levenberg-Marquardt algorithm was used with 23 neurons in the hidden layer with 259 gamma spectra in the input. Because the interest of the study deals with five elements, five neurons representing peak counts of five isotopes in the input layer were used. Five output neurons revealed mass information of these elements from irradiated kidney stones. Results showing max error of 17.9% in APA, 24.9% in UA, 28.2% in COM, 27.9% in STRU type showed the success of neural network approach in analyzing gamma spectra. This high error was attributed to Zn that has a very long decay half-life compared to the other elements. The simulation and experiments were made under certain experimental setup (3 hours irradiation, 96 hours decay time, 8 hours counting time). Nevertheless, the approach is subject to be generalized for different setups.

ACKNOWLEDGMENTS

I would like to express the deepest appreciation to my adviser, Dr. Xin Liu and Nuclear Engineering Department at MST.

As an appreciation, I also would like to dedicate my PhD degree to my father, Mustafa Sahiner, who passed away during preparation of my dissertation defense.

TABLE OF CONTENTS

	Page
ABSTRACT	iii
ACKNOWLEDGMENTS	iv
LIST OF ILLUSTRATIONS	viii
LIST OF TABLES	x
 SECTION	
1. INTRODUCTION.....	1
1.1. ELEMENTS IN BIO-SAMPLES	1
1.2. NEUTRON ACTIVATION ANALYSIS	1
1.2.1. Neutron Source	4
1.2.2. Suitable Reactions	5
1.2.3. Sample Preparation	6
1.2.4. Experimental Setup.....	6
1.2.5. Detectors	7
1.2.6. Data Analysis	8
1.3. ARTIFICIAL NEURAL NETWORK.....	10
1.3.1. Training Algorithms	13
1.3.2. Activation Functions	15
1.3.3. Perceptron Network	16
1.4. REVIEW	17
2. METHODOLOGY	20

2.1. WORKFLOW	20
2.1.1. Identification	20
2.1.2. Quantification	21
2.2. MCNP SIMULATION	23
2.2.1. Neutron Activation Simulation	23
2.2.2. Surface Current (F1) Tally	24
2.2.3. Pulse Height (F8) Tally	25
2.3. CINDER'90	26
2.4. ROOT	27
2.5. IDENTIFICATION	28
2.5.1. Data Preparation	28
2.5.2. Data Analysis	28
2.5.3. Perceptron Network	29
2.6. QUANTIFICATION	30
2.6.1. Experimental Data	30
2.6.2. Simulated Data	31
2.6.3. Neural Network	31
3. RESULTS	34
3.1. IDENTIFICATION	38
3.2. QUANTIFICATION	41
4. CONCLUSIONS	56
APPENDICES	
A. NEUTRON ACTIVATION SIMULATION	60
B. PULSE HEIGHT TALLY SIMULATION	63

C. CINDER'90 INPUT	67
D. MATLAB CODE FOR HIDDEN LAYER SIZES	71
REFERENCES	75
VITA	82

LIST OF ILLUSTRATIONS

Figure	Page
1.1 Nuclear steps of neutron activation.	2
1.2 Gamma spectrum example from APA type kidney stone.	3
1.3 Representation of a single neuron in ANN [1].	12
1.4 Representation of an ANN [1].	13
1.5 Speed and memory dependency of the algorithms.	16
2.1 Flow chart for identification analysis.	21
2.2 Flow chart for ANN analysis of gamma spectra.	22
2.3 Experimental setup for kidney stone samples.	31
2.4 Three-layer Neural Network with 23 neurons in the hidden layer	32
3.1 MCNP F1 tally simulation of delayed gammas from NaCl sample.	34
3.2 MCNP F8 tally simulation of delayed gammas from NaCl sample when no GEB card present.	35
3.3 FWHM function fitting for the parameters.	36
3.4 MCNP F8 tally simulation of delayed gammas from NaCl sample when GEB card applied.	38
3.5 Experimental and simulated gamma spectrum from APA kidney stone.	39
3.6 ROOT analysis of the APA spectrum for background.	40
3.7 Background subtraction from the spectrum.	41
3.8 Confusion matrix for linear perceptron.	42
3.9 Construction for perceptron network representation.	43
3.10 LM error with different number of neurons in the hidden layer.	45
3.11 BR error with different number of neurons in the hidden layer.	46
3.12 SCG error with different number of neurons in the hidden layer.	47
3.13 LM error with different size of training data.	48

3.14 Regression plot for training, validation, and test.	49
3.15 Regression plot for training.	50
3.16 Regression plot for validation.	51
3.17 Regression plot for test.	52
3.18 MSE values during training with purelin function in the output layer.	53
3.19 MSE values during training with logsig function in the output layer	53

LIST OF TABLES

Table	Page
1.1 Commonly used activation functions [2].	19
2.1 Parent and daughter isotopes in simulations.	24
2.2 A portion of training data	29
2.3 Corresponding portion of target data.	30
3.1 FWHM parameters for the GEB card in MCNP.	37
3.2 APA type kidney stone test for identification	44
3.3 External validation of the neural network.	54
3.4 Neural network analysis of experimental spectra for relative error in %.....	54
3.5 Summary of the optimum neural network.....	55

1. INTRODUCTION

1.1. ELEMENTS IN BIO-SAMPLES

With changing nutrition habit, there is an increase in kidney stone diseases [3]. Scientists are interested in explaining the formation of these stones. In recent studies, trace elements were found to be crucial in formation of the stones [4, 5, 6]. Elements that have *mg/kg* or *μg/kg* or less concentration in a human body are called trace elements. Some trace elements play as inhibitors in human metabolism, such as Co, Cr, Cu, Fe, I, Mn, Mo, Se, As, F, Ni, Si, Sn, V. Some of them are toxic, such as As, Be, Cd, Hg, Pb, Se, Tl, Cr, Mn, Ni, Sb, Si. There are more elements that are not classified, such as Ag, Al, Au, B, Ba, Br, Ce, Cs, Ga, Ge, Li, Np, Pt as well as rare earth elements, including Ru, Sc, Sr, Te, Th, Ti, U, W, Zr [7]. In fact, four elements (As, Cr, Mn, Ni, Si) can be found as common elements in inhibitors and toxicants classes. Although the elements are inhibitors, more than an adequate level of them may be toxicants in metabolisms. Thus, precise detection of trace elements is important.

Bio-samples are widely analyzed by chemical techniques. However, nuclear-physics techniques such as X-ray fluorescence analysis and neutron activation analysis are more sensitive in quantifying the amount of these trace elements [8].

1.2. NEUTRON ACTIVATION ANALYSIS

If a neutron is captured by a nucleus, the nucleus becomes unstable because neutron-proton balance is deformed. The nucleus might suffer β^-/β^+ decay or γ decay or both to become stable again. By detecting the activity of the unstable isotope, information about

incoming neutron flux and the parent of radioisotopes can be obtained. This process is called neutron activation analysis (NAA) [9]. Figure 1.1 is a representation of nuclear processes of neutron activation [10].

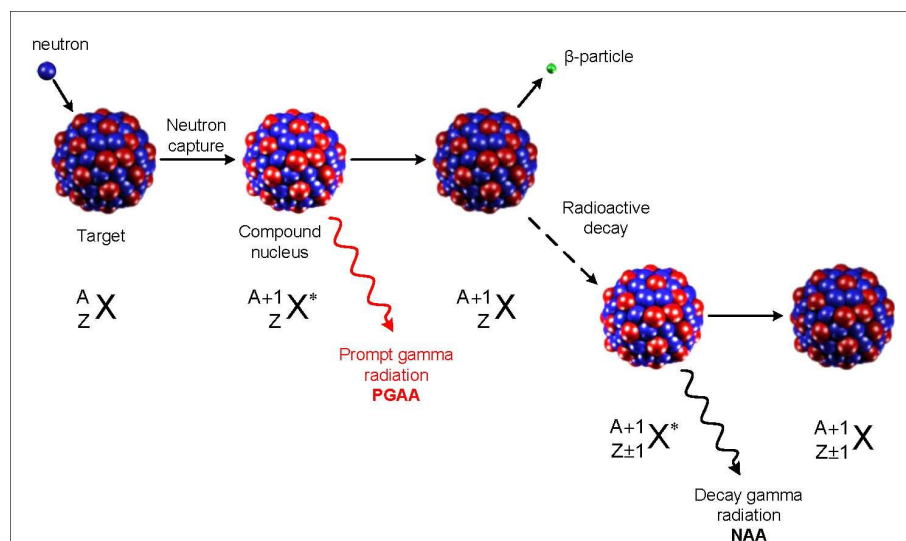


Figure 1.1. Nuclear steps of neutron activation.

The analysis was first used in 1938 for $^{32}\text{S}(n, p)^{32}\text{P}$ reaction to determine sulfur in bio-samples [11]. Neutron activation allows qualitative and quantitative analysis for target nuclei. Analysis can be conducted based on the type of radiation, energy of radiation, intensity of radiation, and half-life of produced radioisotopes [9]. Radiation energy (especially gamma) is characteristic for absorbing nuclei [12]. Analysis of gamma rays, which are emitted immediately after neutron irradiation, is called prompt neutron activation analysis, while analysis after beta decay with some time is called delayed neutron activation analysis [13].

Neutron activation is used for many purposes. Isotope production is one of them and produces radioisotopes for nuclear medicine usage. Highly radioactive waste also can be transformed into less radioactive nuclei through neutron activation. Beside these uses, neutron activation is also used for material analysis as NAA. NAA has a critical role

detecting explosives in safeguard, archeology, forensic science, etc. In this study, analysis of biological samples using NAA was the major focus. Specifically kidney stones were taken into consideration to support formation studies.

Four types of kidney stones (Apatite "APA", Calcium Oxalate Monohydrate "COM", Struvite "STRU", Uric Acid "UA") were received from Mayo Clinic. Identification and concentration analysis of selected elements that were believed to have higher impact on stone formation were analyzed by Sahiner et al [14]. Number of kidney stone samples were not enough to draw a solid conclusion. Nonetheless, results of the analysis were enough to confirm the correlations with the literature. As an example, a positive correlation between Zn and Ca was confirmed as suggested by Srivastava et al and Lin et al [3, 15]. Figure 1.2 is an example of gamma spectrum for 8 hour counting.

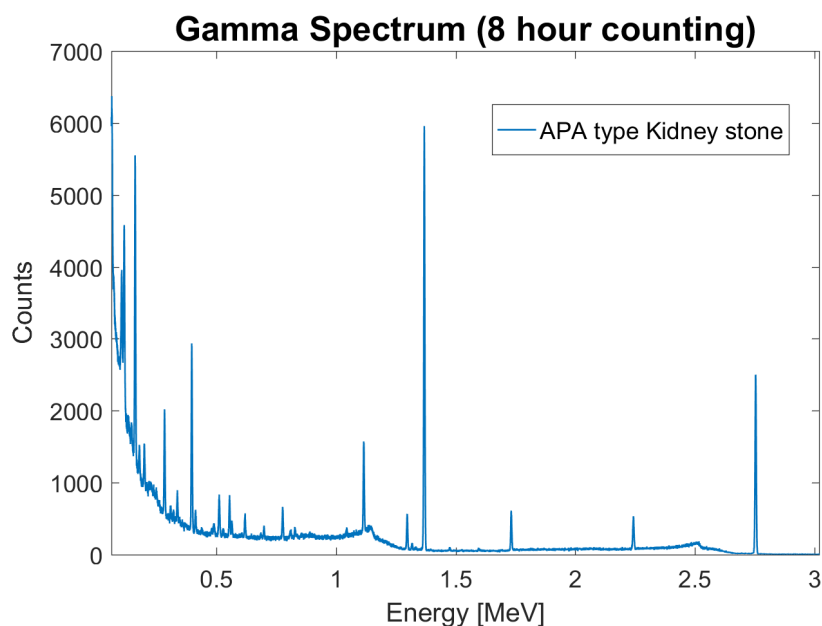


Figure 1.2. Gamma spectrum example from APA type kidney stone.

In neutron activation analysis, there are certain experimental considerations that have high impacts on sensitivity of the measurements. Deviation from optimum choice for the source, suitable reactions, saturation time for activations, detection time, detector types, etc., may cause a loss of information. If an element in a sample was not irradiated long enough, the isotope which is the signature of that element may not appear on a detector.

1.2.1. Neutron Source. In NAA, neutrons are required to cause activation of a sample. The strength of the source determines the attainable activity. Reaction probabilities to activate an irradiated sample differ with energies of incoming neutrons. The interaction probability is due to the binding energy of the target nuclei. Quantum states of the target nuclei causes resonances in interaction probabilities over a range of energy. Neutrons can be classified in two groups based on their energies, either fast neutrons or thermal neutrons. Some sources may use an epithermal category in-between. Thermal neutrons are the neutrons that have energy about 0.025 eV and an average velocity of 2200 m/s [8, 16]. Fast neutrons are able to penetrate through material with a large thickness. Thus, fast neutrons are suitable to activate bulk material [17].

A neutron source to irradiate a sample can be a research reactor, a neutron generator, or an isotropic neutron source. Research reactors are commonly used for research, education, and training purposes. They are usually the most suitable neutron source for NAA due to high neutron flux $\approx 10^{10} - 10^{15} ns^{-1} cm^{-2}$ in the reactor core [18, 19]. Neutrons including prompt neutrons and delayed neutrons are produced by fission reactions in nuclear reactors. They have energies ranging from the thermal level of few meV to the relativistic level of ≈ 20 MeV [20]. This wide energy range may result in complex gamma spectra from an irradiated sample.

Neutron generators are compact in size and can manage neutron flux up to $10^{11} s^{-1} cm^{-2}$. They are commonly employed for radiography and neutron activation [21]. Neutron generators produce neutrons by fusion reactions, such as Deuterium-Deuterium (DD) reaction, Deuterium-Tritium (DT) reaction, and Tritium-Tritium (TT) reaction. DD

generators produce almost monoenergetic neutrons with 2.45 MeV. Similarly, DT generators are able to generate ≈ 14 MeV monoenergetic neutrons. With the disadvantage of lowest relative intensity, TT generators have wider spectrum between 0-10 MeV [22].

Isotropic neutron sources are another type of neutron sources. This include (n, α) reactions such as an alpha emitter embedded with Boron or Beryllium. This reaction produces neutron flux about $10^6 ns^{-1} cm^{-2}$ with an energy range from 2.4 MeV to 4.5 MeV. The source strength is subject to decay over time. A spontaneous-fission source such as californium is also subject to produce neutrons [19].

Overall, the choice of neutron source can be made by reaction selection based on a specific purpose. These sources have advantages and disadvantages depending on the required flux and energy (monoenergetic or spectrum). As an example, some of the light elements cannot be detected through classical NAA unless 14 MeV neutrons are used [22].

1.2.2. Suitable Reactions. Selection of the reactions is dependent on the choice of neutron sources as well as target samples. Fast neutrons may lead to interference reactions because they may interact with matters through endothermic reactions with a few exceptions. As an example, fast neutrons may interact with aluminum via $^{27}Al(n, p)^{27}Mn$, $^{27}Al(n, \alpha)^{24}Na$, $^{27}Al(n, \gamma)^{28}Al$. If there is silicon in irradiated material, $^{28}Si(n, p)^{28}Al$ reaction is possible. Both ^{27}Al and ^{28}Si result in ^{28}Al radioisotope. This may cause false analysis. Furthermore, radiative capture (n, γ) of thermal neutron interaction with target nuclei is a dominant reaction because (n, α) reaction is endothermic with a few exceptions. Radiative capture reaction is possible with all nuclei without threshold energy. Its cross-section is usually higher for thermal neutrons than fast neutrons [9]. Both (n, α) and (n, p) reactions are endothermic reactions with energy of 1-5 MeV. Neutron multiplication $(n, 2n)$ reactions are also endothermic with energy of about 10 MeV and higher [12]. Absence of interfering reactions improves the sensitivity and accuracy of the gamma spectra. Depending on the choice of the reaction, thermal neutrons can be filtered by using neutron absorbers in either sample capsule or reactor channel that is installed permanently. Cd ($\sigma_{th} = 199910b$)

and ^{10}B ($\sigma_{th} = 3838\text{b}$) are commonly used absorbers in NAA. Neutron cutoff energy 0.55 eV can be provided by 1 mm thick Cd sheet. This allows only fast neutrons to pass through the absorber. Finally, most of the trace elements in human body are detectable through (n, γ) reaction [8, 12].

1.2.3. Sample Preparation. Samples to be irradiated should be prepared with care because neutron activation is very sensitive. Hand contact may contaminate the sample by introducing enough amount of human sweat that contains sodium and chlorine. Dry boxes and a clean room with clean tools are necessary during sample preparation. Samples can be prepared in solid form (larger piece or powder) or liquid form. Samples must be measured for mass accurately [9]. A small amount of the sample due to high activity might cause exposure risk. In this case, a homogeneous solution might be prepared. Afterwards, a portion of the solution can be taken to contain a very small amount of the sample. A small amount of the solution will contain a smaller amount that is not directly measurable with sensitive weight measuring devices. In order to use this preparation, the sample should be soluble. An example of this is a salt sample. As sodium might cause high activation for a long irradiation time, a small amount can be adjusted. High activation is a disadvantage for the detector causing a large amount of dead time.

1.2.4. Experimental Setup. For experimental setup, there are certain cautions to be taken. Irradiation time, decay time, and counting time have important effects on detection. As an example, if irradiation time is not long enough, then some of the elements that have a small amount of reaction with neutrons may cause a gamma signal to be lost in the background of a spectrum. Similarly, longer decay time may cause loss in detecting short half-life radioisotopes [14]. After a long irradiation, samples may have high reactivity level that will result high dead time in detectors as well exposure for technicians. Preliminary activity measurements with a counter can be helpful for choosing decay time. High activity decay away in this time period such that detectors can measure gamma rays with a negligible dead time. The decay time reduces the exposure rate of the sample. Then the technicians

can handle the irradiated sample within allowable radiation dose limit. Although there are automated hydraulic systems to transfer samples from where they are irradiated to where they are measured, the use of the systems is not wide. Additionally, shorter detection time results a spectrum that is dominated by radioisotopes that have shorter half-life. Likewise, longer detection time results a spectrum that is dominated by radioisotopes that have longer half-life.

1.2.5. Detectors. The use of various detector sizes and types is significantly important for sensitivity, resolution, and efficiency. The desired detector capability is to be highly efficient with maximum energy resolution. However, the detector choice is in-between sodium iodine (NaI) detectors and high purity germanium (HPGe) detectors. While NaI detectors have high efficiency, HPGe detectors have high energy resolution [9, 16]. The choice is a trade-off for a primary purpose. If irradiated sample results in a simple gamma spectrum (a few separate gamma peaks), the choice can be made for efficiency by using NaI detector. In contrast, if a sample results in highly complex gamma spectrum, then the high energy resolution is necessary to distinguish gamma peaks. The stone samples from the human body generate highly complex spectra [14]. Therefore, an HPGe detector gives higher energy resolution (2 keV).

During prompt neutron activation analysis, the detector crystal is subject to be damaged by high neutron flux. For this purpose, n-type HPGe detectors are suggested because they are less sensitive to neutron damage than p-type.

As an addition to the detector choice, the standard electronics are capable of collecting data with negligible error [12]. Detector response cannot be as fast as electronic signals. There is a time limit for all detectors to separate two events. This time limit is called "dead time" and is different for detector types. This dead time ranges from microseconds to milliseconds. Since dead time caused by electronics is so small (10^{-7} second) compared to detector dead time, "dead time" refers to detector dead time only. If there is large dead time loss in the spectrum, there must be a dead time correction to obtain true counts from the

spectrum [9, 16]. There is no exact representation of dead time despite the fact that good models exist in the literature. These models consist of paralyzable model or non-paralyzable model or combination of both.

1.2.6. Data Analysis. Data analysis is classified into two categories as quantitative and qualitative analysis. Qualitative analysis is mainly for identification of parent elements in irradiated sample through their daughter products with characteristic gamma rays in a spectrum. Quantitative analysis is more detailed analysis to calculate element concentrations in the sample through obtained spectra [13].

Although data analysis can be made manually, analytical software is very helpful for specific purposes. Especially in identification, it gives start-up suggestions. When analysis with a commercial software is made, peaks might be labeled with all possible radioisotopes. Some of the radioisotopes that have a very short half-life, in reality, may not survive over long decay and counting time. Nevertheless, software still labels impossible choices on gamma spectra. ^{82}Br and ^{82}Rb have several overlapping gamma peaks. While ^{82}Rb has a short half-life (1.2 min), ^{82}Br has a long half-life (35.3 hour). Although ^{82}Rb would not survive for long decay and counting time, commercial software may result in labeling ^{82}Rb as well as ^{82}Br on spectra. Since the software does not know the experimental setup to rule out all the possibilities, using it might be a good start, but not an actual result. Humans can identify and simplify the identification by taking irradiation time, decay time, counting time, natural abundance, half-life etc., into account. As an example, short-lived isotopes decay quickly and do not survive for long decay times and long counting times.

Due to penetration ability of fast neutrons in a bulk material, the neutrons are able to activate thick targets. Even though thick material causes a self-shielding problem, it has an advantage when only identification of elements is the concern [17].

Identification analysis can be made by finding the peak gamma energy and cross-checking with a pre-developed table. One good source can be found in [23] for identification purposes.

Quantitative analysis is more complicated. This consists of peak information into a formulation. Equation 1.1 allows necessary calculation to find the mass of interest. In Equation 1.1 P_k is net counts under the peak, A_i is atomic mass of the element of interest, λ_{i+1} is decay constant of radioisotope produced, $\epsilon(E_k)$ is absolute full-energy detector efficiency, e_k is probability of photon emission, a_i is atomic abundance of element with A_i , N_A is the Avogadro number, σ_i is cross-section that makes the reaction, t_0 is irradiation time, and $(t_2 - t_1)$ is counting time. In essence, Equation 1.1 summarizes the precision of mass calculation. Error in the parameters propagates through the mass calculation as well. Determining these parameters accurately affects the final mass calculation through error propagation [9].

$$m = \frac{P_k A_i \lambda_{i+1}}{\epsilon(E_k) e_k a_i N_A \sigma_i \phi (1 - e^{-\lambda_{i+1} t_0}) (e^{-\lambda_{i+1} t_1} - e^{-\lambda_{i+1} t_2})} \quad (1.1)$$

Very precise mass calculations can be done by comparing a standard sample with known material. Known sample means known mass and content. Sometimes known samples are referred as standard samples. When known and unknown samples are irradiated under the same experimental condition, all terms in Equation 1.1 for the same isotopes cancel out. Only peak counts are left, as in Equation 1.2.

$$\frac{m}{m_{standard}} = \frac{P_k}{P_{Standard}} \quad (1.2)$$

In the end, the only error source is from net counts under the peaks. However, this is not always the case because elements in the sample of interest are unknown. In other words, the standard sample may not contain the same elements with the unknown sample. This approach requires preliminary analysis. To do the most accurate analysis, an unknown sample should be irradiated for identification. Known samples can be chosen based on the results of the preliminary analysis. The standard sample which contains the same elements can be irradiated under the same setup. Then, the analysis will have very precise results.

Furthermore, the work required for precise results is not always favorable. It requires very good calibration of a detector, very precise mass measurement of the standard sample as well as the unknown sample, and very precise neutron flux distribution. Detector should be calibrated throughout the spectrum range. Experiments should be made under the same conditions where the calibration was made. Calibration is affected by detector temperature, applied voltage, and gain settings. Sample preparation is another challenge due to the facts that are explained earlier. A precise measurement for a very small sample is not possible due to measurement device capability and susceptibility to humidity. Detector resolution and efficiency is a further concern during analysis because efficiency and resolution is not a linear response of a detector. The response is different throughout the spectrum for every energies. The analysis made by commercial software may require elimination of impossible elements such as rare earth elements or very short half-life isotopes. Therefore, researchers look for more practical solutions for the same or better precision.

1.3. ARTIFICIAL NEURAL NETWORK

With the increasing computer technology and mathematical algorithms, scientists tend to use computers to solve complex problems that are not possible to solve by hand. Some of the complex real-life problems can be represented by linear functions or non-linear functions or a combination of both. Not all of the real-life problems can be represented mathematically. Nevertheless, researchers might have input corresponding to an output data set of a system. In this case, computers with improved algorithms can reveal similarities or correlations between input parameters and corresponding outputs. Making computers to adapt or modify their responses based on the known input and output data can be called "Machine learning." Machine learning has become an attractive technique to researchers. Different learning algorithms offer solutions to a variety of problems. Supervised learning is one of the algorithms used most often, whereas unsupervised learning, reinforcement learning, and evolutionary learning are used depending on the problem type. The choice

depends on deciding how the computers are learning to improve results for a given task. In supervised learning, the computer trains itself through a known set of input data with corresponding outputs of a system. In unsupervised learning, target data is not provided to the machine. Instead, the machine finds similarities in the input to categorize the input data [24].

Machine learning has many approaches, such as boosted decision trees, supported vector machines, radial basis functions, multivariate analysis, etc [25, 26]. Artificial neural network (ANN) is another class of machine learning. It solves problems in engineering, science, mathematics, economics and many other disciplines. ANN mimics how the human brain works. The human brain learns things from experience. For instance, babies start learning objects by touching to decide soft or solid, hot or cold. Toddlers learn smell, shape, and color of the objects for identification. Learning is carried out by neuron cells (10^{11} elements) and their connections (10^4 connections per element). The signals from human receptors pass through chemical processes in-between neurons. Although this process is slow compared with electronics, the main advantage of the human neurons is so many connections. When a neuron receives signals from neighboring neurons, the signals are summed and passed through a threshold. If the signal is higher than a threshold, then the neuron fires a signal towards next connections. If not, the signal is not passed.

Some sources may refer to training as "learning process." ANN is a mathematical representation of this process. Whereas a small size ANN can be calculated by hand, a larger size ANN that has so many connections and features requires computers. Figure 1.3 shows a single neuron with incoming connections. The activation function is the threshold for the summed signal to decide whether the signal passes or not. During the learning process, ANN finds the correct weights in-between connections. Correct weights mean the weights that result minimum error between known outputs and calculated outputs. Once the weights are found, the neural network can analyze an unknown input [2, 27].

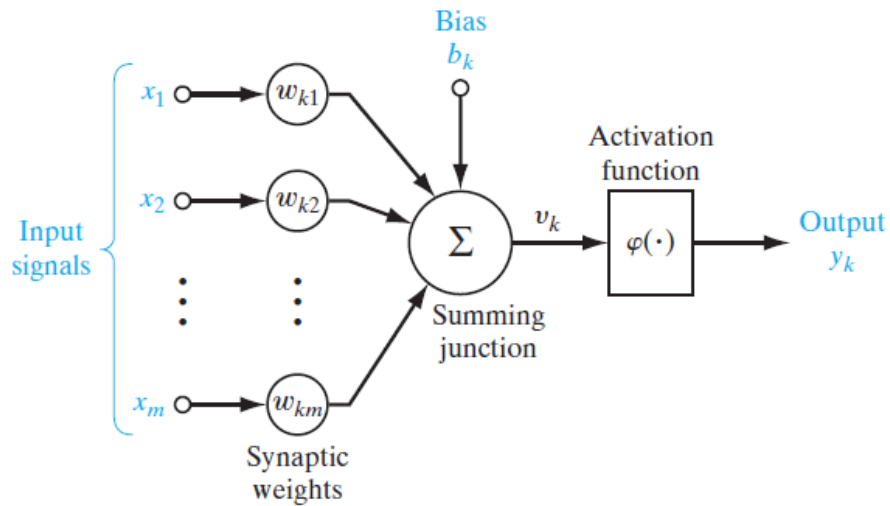


Figure 1.3. Representation of a single neuron in ANN [1].

Usually an ANN contains one input layer, one or more hidden layers, and one output layer. In these layers, there might be one or more neurons. There is no solid guide for a neural network structure because it is problem-dependent. The number of neurons in the input layer and output layer is externally constrained by the problem. Figure 1.4 represents a sample neural network that has 10 input neurons in the input layer, 4 neurons in the hidden layer, and 2 neurons in the output layer with their connections. The sample networks find the weights of the connections with known input and output.

Adaption of a constant threshold to a neural network can be made as an additional input in a layer. This additional weight is called "bias." With a bias, initial weight vector size increases by one. A neural network can be constructed with or without a bias. However, addition of a bias is suggested for better results. For instance, neural networks may result zero outputs for zero inputs. That is not desirable. To overcome this problem, biases are used as a mathematical trick. The biases have a constant value of one.

The biggest time consumption occurs during training. Once the neural network is trained, it gives an instant response regardless of problem complexity [2, 27].

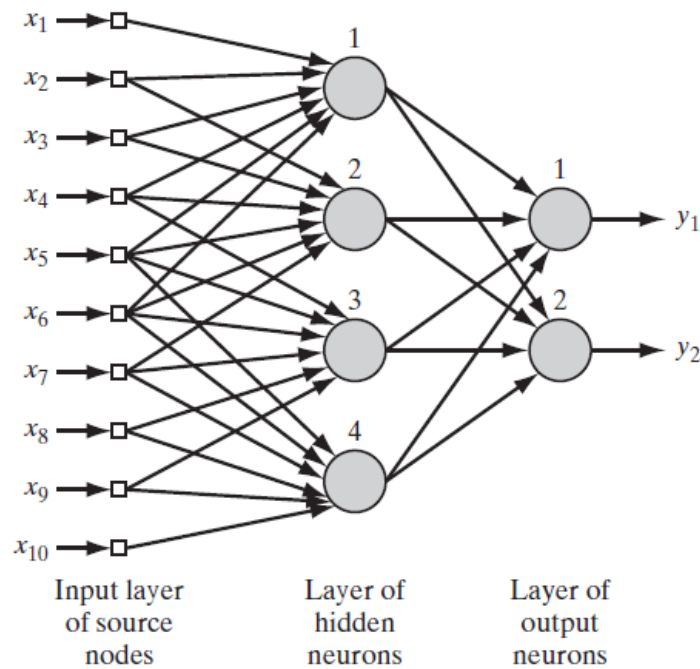


Figure 1.4. Representation of an ANN [1].

1.3.1. Training Algorithms. During training (learning), the neural network updates the weights based on a performance function to the direction where the gradient decreases the most. The standard performance function is usually mean squared error (MSE). The neural network finds optimum weights when this error is minimized. Minimization of MSE is validated by the gradient of the performance function. Training data is usually divided to train, validate, and test the network.

Simply, the neural network iterates Equation 1.3 for converged weights between neurons (nodes):

$$x_{k+1} = x_k - \alpha_k g_k \quad (1.3)$$

Where x_k is vector of current weights, g_k is current gradient, α_k is learning rate. Training algorithms use either gradient or Jacobian methods to reduce the error in the iteration process. Equation 1.3 is an example for gradient descent method. The choice of training algorithms depends on the complexity of the problem, targeted error, problem type (regression or pattern recognition), and number of data points [2].

In order to find the correct weights between connections, there are several algorithms. For testing gradient and the Jacobian approach, the focus was narrowed down to three algorithms. Levenberg-Marquardt (LM) algorithm, and Bayesian regularization (BR) are the most common algorithms. The Scaled conjugate gradient (SCG) algorithm is gaining popularity in addition to the two algorithms.

The LM algorithm uses a numerical approach to find weights. LM is also known as the fastest algorithm in many cases. However, it is found to be less efficient for large networks due to memory requirements for the Newtonian approach. This algorithm is used for nonlinear regression problems rather than pattern recognition problems.

Since LM is the Newtonian approach for performance index, which is a sum of squares function, the final equation for the algorithm has a form of Equation 1.4:

$$x_{k+1} = x_k - [\mathbf{J}^T(x_k)\mathbf{J}(x_k) + \mu_k\mathbf{I}]^{-1}\mathbf{J}^T(x_k)\mathbf{v}(x_k) \quad (1.4)$$

\mathbf{J} is Jacobian matrix, x_k is vector of weights, $\mathbf{J}^T\mathbf{J}$ is Hessian matrix, \mathbf{v} represents the error, \mathbf{I} is identity matrix μ is a parameter to avoid an invertible problem in the Hessian matrix. If μ is decreased to zero, the algorithm becomes the Gauss-Newton approach.

Bayesian regulation uses a probabilistic approach to minimize the performance index. According to Bayes' theorem, if there are two random events (A and B), conditional probability that one event occurs is represented with Equation 1.5.

$$P(A|B) = \frac{P(B|A)P(A)}{P(B)} \quad (1.5)$$

Starting with the theory, BR assumes the weights are random and distributed with Gaussian distribution. Since it is a probabilistic approach, BR algorithm prevents the over-fitting problem. The over-fitting problem may be caused by a use of too many neurons in the network. When the BR algorithm is used, validation data is not needed. For high amounts of training data, BR and LM result in the same error since one approach is numerical and the other is probabilistic [2].

In addition to the previous two methods, the SCG method is preferable for a large data set due to small memory requirements. The SCG method is efficient for large networks for pattern recognition. This algorithm is a modified version of conjugate gradient, which works only for positive definite value of the Hessian function. Equation 1.6 estimates the term \mathbf{s}_n for non-zero input quantity $x_n = \mathbf{p}_n^T \mathbf{s}_n$.

$$s_n = \frac{E'(\tilde{w}_n + \sigma_n \tilde{p}_n) - E'(\tilde{w}_n)}{\sigma_n} - \lambda_n \tilde{p}_n \quad (1.6)$$

\mathbf{p} is non-zero weight vectors, \mathbf{E} is error function, λ is adjusted scaler in each iteration to find estimated term, and σ can be a positive value very close to zero. SCG is validated by first degree of the gradient while LM is validated by second degree of the gradient as in Jacobian. As a result, SCG linearly converges faster than the other standard gradient methods [28].

Since there is no solid guide for ANN systems, determining the best algorithm for a specific purpose is important. the guiding information above might be helpful to choose the better algorithm based on the problem type. As the focus is not to improve any algorithms, the information was held brief with enough information to compare them. More detailed information can be found in [1, 2, 28]. Figure 1.5 summarizes speed and memory dependency of three algorithms.

1.3.2. Activation Functions. In the definition of a single neuron, the sum of weighted inputs are passed through an activation (transfer) function. Activation functions form the output of a neuron. Thus, for the output layer, the choice of the activation

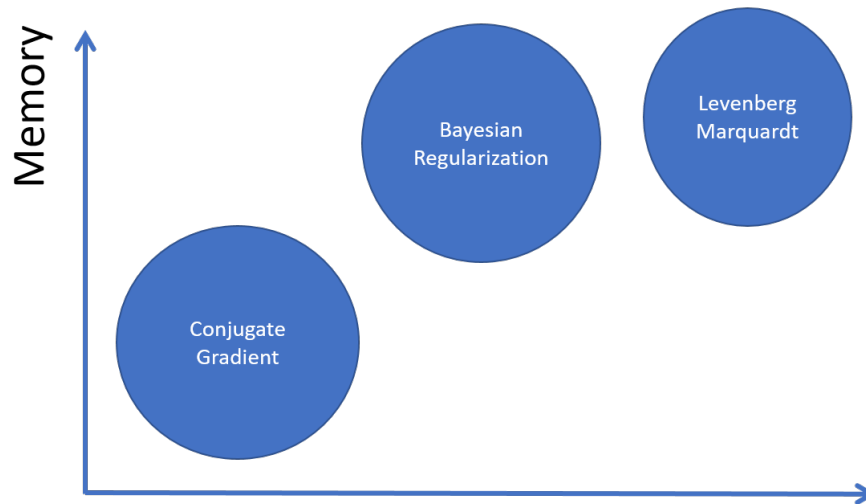


Figure 1.5. Speed and memory dependency of the algorithms.

functions is semi-dependent on problem specifics. The most used activation functions are tabulated in Table 1.1, though users can choose their own functions—either linear or nonlinear. Feedforward networks use linear activation functions, while backpropagation networks use smooth differentiable functions. Moreover, the choice of activation functions for a hidden layer might require care. The logistic (sigmoid) function, which results in interval of $[0,1]$, may cause systematic bias [1, 2]. A feedforward network calculates output from input in one pass. Backpropagation calculates the derivations in the last layer and propagates the derivatives backward with chain rule. Backpropagation is used for multilayer networks.

1.3.3. Perceptron Network. While a network can be very complex with multiple layers to solve complex problems, it can also be a very simple layer network called "perceptron." A perceptron network can solve a very narrow range of problems, usually classification problems. A perceptron network is an old ANN. It started to be used in pattern recognition problems. However, it did not solve pattern recognition problems that

were not linearly separable. Nonetheless, it still solves classification problems powerfully. A perceptron network uses the hard limit as a transfer function and perceptron learning. During learning, the perceptron network solves correct weights in Equation 1.7:

$$a = \text{hardlim}(Wp + b) \quad (1.7)$$

\mathbf{a} is the output of the network, \mathbf{W} is a weight matrix, \mathbf{p} is the input, \mathbf{b} is the bias. In Equation 1.7, hardlim function results in one if inner product of \mathbf{W} and \mathbf{p} is greater than or equal to $-b$. If the product is less than $-b$, it results in zero. The network separates input space into two region with a decision boundary. Perceptron network guaranties convergence with finite number of iterations if the solution exists [2, 29]. A perceptron network can be constructed as one layer or multilayer network. However, for the focus of this study, one layer perceptron network can solve the linearly separable binary condition for identification. Therefore, details for multilayer perceptron is excluded here.

1.4. REVIEW

Artificial neural network has been used by few researchers for neutron activation analysis. While the main use of NN was identification [30, 31, 32, 33, 34], it was employed for detection of explosives [31, 35, 36], drug [35], uranium [37], radon contamination [38]. The NN was also used to determine cement concentration [39, 40] as quantification analysis. Besides these research, gamma spectra unfolding [30], uncertainty estimation in gamma spectra [41], interaction identification [42], anomaly detection in gamma spectra [43], fast neutron spectra detection [44] were analyzed by artificial neural network.

Matlab, NeuroShell, Neuroph, QuickNet were commonly used artificial neural network toolboxes or software. Simple structures with a few neurons in layers as well as complex structures of number of neurons in layers were employed. Sigmoid, tansig transfer functions were used in identification problems. Variety size of training data were reported.

Although small size of training data might be enough for identification or detection purposes, larger training data size was required for quantification purpose. This was concluded due to high relative error (3-12% by [39], 5-9% by [44], 14.5-49.7% by [33]) reported on quantification analysis.

Training data for these neural networks has been prepared by Monte Carlo (MC) simulations (MCNP and Geant4) [30, 31, 32, 33, 34, 36, 37, 38, 40, 45, 46, 47] and experiments [32, 35, 37, 39, 41, 44, 48].

Some of the previous works have reported preparation of training data by simulation and analysis of simulated cases. Even though simulations have an advantage to generate large size of synthetic data, simulations do not represent real life detections. Some other previous works have reported preparation of training data by experiments and analysis of experimental data. As quantification analysis require very large training data (the suggested size is reported in the result section of this thesis), experiments to prepare required size of data would take months for a research reactor depending on availability of it. If it is an institutional reactor for educational purposes, because of the availability, data preparation will be extended to years. Due to the change of environment temperature, reactor core behavior, detector conditions, etc., experimental setup will differ. Therefore, extra error conditions will be added.

In order to cope with the disadvantages mentioned above, a new approach to neutron activation analysis was conducted. The approach includes training the neural network with simulated data that is large in size and analysis of experimental data.

Table 1.1. Commonly used activation functions [2].

Function Name	Input-Output Relation
Hard Limit	$a = 0$ when $n < 0$ $a = 1$ when $n \geq 0$
Symmetrical Hard Limit	$a = -1$ when $n < 0$ $a = +1$ when $n \geq 0$
Linear	$a = n$
Saturating Linear	$a = 0$ when $n < 0$ $a = n$ when $0 \leq n \leq 1$ $a = 1$ when $n > 1$
Symmetric Saturating Linear	$a = -1$ when $n < -1$ $a = n$ when $-1 \leq n \leq 1$ $a = 1$ when $n > 1$
Log-Sigmoid	$a = \frac{1}{1+e^{-n}}$
Hyperbolic Tangent Sigmoid	$a = \frac{e^n - e^{-n}}{e^n + e^{-n}}$
Positive Linear	$a = 0$ when $n < 0$ $a = n$ when $n \geq 0$

2. METHODOLOGY

Methodology of the work was divided into identification and quantification analysis of gamma spectra. Although the main focus was quantification analysis, identification analysis with neural network approach was made to avoid occurrences of elements due to error margins from the neural network in quantitative analysis.

2.1. WORKFLOW

2.1.1. Identification. Identification of a spectrum was not primary focus of the study. However, this work contributed quantification analysis. As ANN has associated errors, they might result in elements being present with a very small fraction from the spectrum although they are not there. Therefore, identification analysis was done before conducting the ANN for quantification analysis. Figure 2.1 shows the steps of identification analysis.

This problem could be reduced for classification problem by generating 32 cases (different combinations) of 5 elements. Five elements and 32 cases were represented in binary form to train the perceptron network for classification. Classification term in ANN was used for identification term in NAA. Monte Carlo simulation and CINDER'90 were used to generate gamma spectra to simulate extreme cases. The extreme cases were assumed to be a very small and very large Gaussian energy broadening in the electronic signal, shift in gamma spectra due to gain settings, a very small concentration of elements, and a very small peak in the spectra. TSpectrum that is a ROOT [26] object was employed for peak search and generation of results as a text file format. Both ROOT peak search results and target data were prepared in binary format resulting in 1 if peak was found, 0 if not. Five

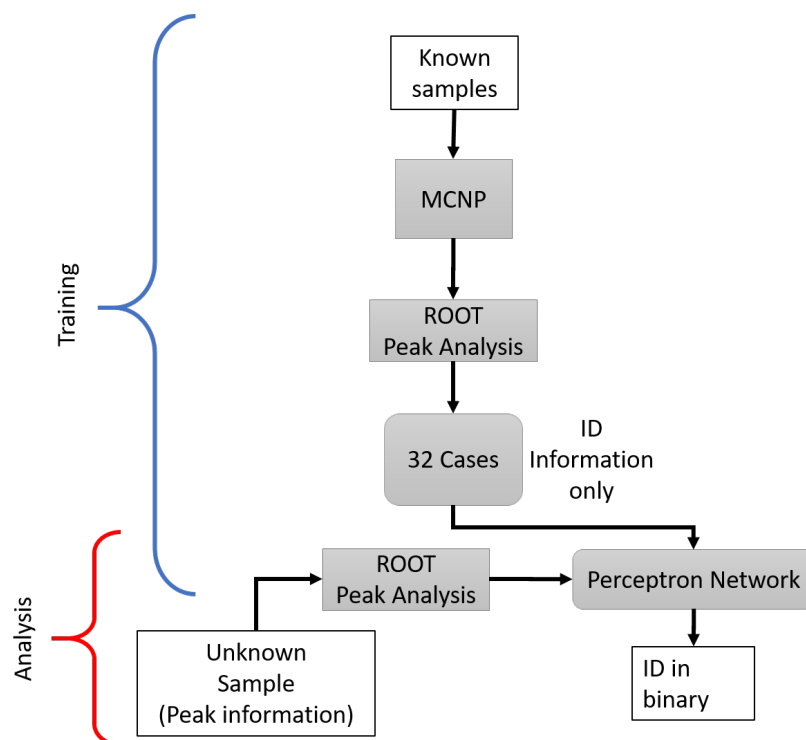


Figure 2.1. Flow chart for identification analysis.

elements after neutron irradiation were searched for 13 unique gamma rays (four from Na, six from Br, one from Zn, one from K, one from Au). ROOT codes to analyze a spectrum is open-source and available online.

2.1.2. Quantification. Neural network analysis of gamma spectra consists of data preparation, feature extraction from the data, calibration of prepared features, training, and analysis of unknown samples. Figure 2.2 describes the flow chart of the system. Four types of kidney stones including APA, COM, STRU, UA type were received from Mayo Clinic for NAA. A Salt (NaCl) sample with known mass besides kidney stone samples was prepared for irradiation. The same experimental setup was used to produce simulated data in order to train a neural network. Since Monte Carlo simulation assumes perfect conditions, a correction between experimental data and simulated data was required. Rather than introducing a whole spectrum into a neural network, peak features were obtained from

the spectra. This can be done either manually or by using peak finder codes available in MATLAB [29] or ROOT software. Correction factors for each energy bins are obtained by comparing peaks from known mass and simulated spectra. Then, determined correction factors were used on unknown samples. The Correction factors are energy dependent since they implicitly depend on detector efficiency, which is energy dependent as well. After preparation of data, a neural network can be structured and trained. As there is no solid guide to prepare a neural network for specific applications, different training algorithms, number of neurons in a hidden layer, and size of training data were compared to choose the one fits the needs best.

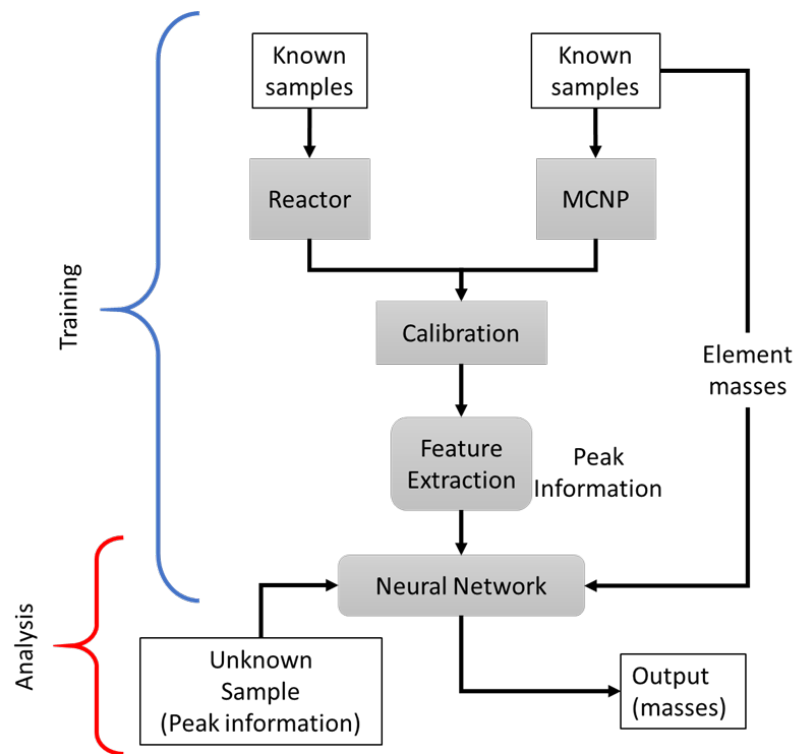


Figure 2.2. Flow chart for ANN analysis of gamma spectra.

2.2. MCNP SIMULATION

Monte Carlo N-Particle transport code (MCNP) is a Monte Carlo technique to solve transport equation. It is distributed by Radiation Safety Information Computation Center (RSICC). Tallies in MCNP provide history of particles during nuclear events that are in terms of current, flux, and pulse height. Tally outputs can also be modified during simulation for dose and energy in a medium [49].

2.2.1. Neutron Activation Simulation. Newly introduced ACT card in MCNP 6.1 makes it possible to simulate neutron activation for emitted prompt and delayed gamma rays. It is possible to simulate these gamma rays as multigroup or lines. Multigroup simulation is limited in 25 bins currently. Even though the limitation exists, the results allow good prediction for gamma dose analysis and speed in consecutive simulations [50]. Line emission data can be used in material identifications [14].

Real life neutron activation for prompt and delayed gamma simulation consists of two consecutive simulations as if a sample is irradiated and moved to a detector to measure gamma emission. To simulate both cases, MCNP provides results of the first simulation as a source definition to the second simulation. SSW card in MCNP stores the results in a separate file named as wssa. SSR card in MCNP simulation of latter reads the source definition from wssa file once it is renamed as rssa. In the prior simulation, time card can be used to simulate for demanded irradiation time, decay time, and measurement time [49, 50]. However, the disadvantage of SSW is that it does not store time dependent information. Instead, it stores all designated particles of all time in the current MCNP release. Manually, the results can be analyzed to prepare fixed source for the next simulation.

The only limitation to simulating NAA with MCNP is due to the data library. MCNP does not have a data library for some of the isotope decay products. Those isotopes usually have with very short decay half-life. Nonetheless, those isotopes are not a concern in this study.

Table 2.1. Parent and daughter isotopes in simulations.

Natural Element	Radioisotope	Half-life
Na	Na-24	14.9 h
Br	Br-82	35.3 h
K	K-42	12.4 h
Au	Au-198	2.7 d
Zn	Zn-65	244.3 d

By finding common isotopes in kidney stones, four elements (Br, Na, Au, K, Zn) were selected for simulation. Primary reaction of these elements is thermal capture given in Table 2.1. In order to simulate multiple delayed gamma spectra, mass concentration of five selected elements were produced. A set of 260 mass concentrations was randomly generated. Concentrations were used in input files for MCNP simulation within a material card. Delayed gamma energies were simulated in the form of lines by using the ACT card. The neutron source was modeled as a beam to irradiate the samples.

2.2.2. Surface Current (F1) Tally. Surface current (F1) tally was used to simulate delayed gamma lines. MCNP simulation results for perfect conditions. Therefore, a correction between simulated results and experimental measurements was required. If terms in Equation 1.1 are divided into two groups, one group combining the exponential decay terms, and the other group combining the rest of the terms, correction is to relative ratio of the counts. As detector response would be different at different energies, the correction had to be energy dependent and calculated accordingly.

2.2.3. Pulse Height (F8) Tally. Pulse height (F8) tally is used to mimic real detector response. It is used to simulate photon and electron interactions with detectors. With neutrons, it does not work well because of its non-analog nature. With analog capture, particles are killed with the probability of capture. On the contrary, in non-analog (implicit) capture, particles are not killed immediately. Instead, their weights are reduced. The latter does not represent the actual neutron capture interaction. Therefore, F8 tally works with implicit capture to represent real detectors for photons and electrons for a better variance. Pulse height tally cannot be directly used with time bins to simulate time-dependent detector response. The work around this type of problem is to use energy deposition tally (F6) with time bins and feed in F8 tally.

In order to simulate a detector response, F8 tally offers unique features such as GEB (Gaussian energy broadening) [49]. With this function, it is possible to simulate broadened signal in the detector caused by electronics of the detector. The GEB card can help to simulate broadening with either build-in detectors or custom detectors. Simulation for custom detectors requires calculations of Full width half maximum (FWHM) function parameters in Equation 2.1.

$$FWHM = a + b\sqrt{E + cE^2} \quad (2.1)$$

Where E is the energy of incoming particles, and a, b, c are parameters used in the GEB card to represent a custom detector response [46, 49, 51].

From kidney stone spectra, FWHM distribution can be driven by fitting spectral features (energy and FWHM) to the Equation 2.1. These parameters were used in the GEB option to represent broadening similar to that one of HPGe used to obtain the experimental data. As annihilation, single escape, and double escape peaks are affected by particle

interactions resulting in different tailing, they do not represent actual detector behavior. Thus, in the GEB calculation, these peaks were not used. The detector consists of planar geometry germanium crystal. A similar geometry that Fantinova [52] reported was used.

In order to produce gain for different settings, Equation 2.2 was used.

$$Energy = Shift + Gain * Channel \quad (2.2)$$

2.3. CINDER'90

CINDER'90 is a code which dates back to 1960 to calculate inventory of irradiation of a sample. The inventory contains atom density and activity of nuclei over time by destruction and production rates. Based on the purpose, it is also referred as activation code or transmutation code. The code carries the density calculations with the Markovian chains algorithm to solve the differential equation in Equation 2.3.

$$\frac{dN_m(t)}{dt} = -N_m(t)\beta_m + \bar{Y}_m + \sum_{k \neq m} N_k \gamma_{k \rightarrow m} \quad (2.3)$$

$N_m(t)$ is atom density at time t , β_m is total transmutation probability of nuclide m , \bar{Y} is production rate, $\gamma_{k \rightarrow m}$ is the probability of nuclide k transmuting nuclide m . Solving the differential equation in CINDER'90 is possible for 3400 nuclides with $1 \leq Z \leq 103$. The code works only with 63 multigroup neutron flux with energy of $E_n \leq 20 MeV$. CINDER'90 simulation requires working MCNPX [53]. MCNPX is the Monte Carlo code to simulate charge particle interactions. The current Monte Carlo code was combined for all particles in MCNP with 6.1 version.

Due to the demand for an automated system in gamma spectroscopy with reduced human error, this study has been conducted. Current use of ANN in gamma spectroscopy includes training with simulated data and analysis of simulated spectra or training with experimental data to analyze experimental data. The disadvantage of the former is that the

simulation does not correspond to experimental results due to impurities in detecting. The latter also has a disadvantage in obtaining experimental data. To obtain a large data set for training purposes requires a very long use of the neutron source if detection of long half-life isotopes is a concern. To eliminate these disadvantages, the focus is to use simulated data for training in order to analyze experimental data.

This study has a focus on analysis of trace elements in bio-samples. However, it can be generalized by changing the experimental and simulated data to another setup with relevant changes in Equation 1.1.

Before using the pulse height (F8) Tally, Cinder'90 code was used to obtain the highest number of isotopes produced for 8 hours measurement after irradiation. The highest amount was obtained from thermal reaction ($n, \hat{I}\hat{s}$) for the natural elements. The ratios of the isotopes were used in F8 tally simulation of HPGe detector as source definition.

2.4. ROOT

ROOT is an object oriented scientific software. It has been widely used by particle physicists to deal with large data. ROOT makes data processing, statistical analysis, visualization and storage of large data possible where equivalent software struggles. ROOT is well known with frequent updates as a consequence of being open source code. A large number of scientists contributes to the coding. Although, the software has been written in C++, some other languages (Python and R) have been integrated. This feature is very useful for pre-processing or post-processing.

TSpectrum is a class of spectrum analysis function. This class can perform background estimation, deconvolution, smoothing, peak searching, and fitting of a spectrum [26]. It was found to be best to estimate Compton background in a spectrum.

TSpectrum can be used to locate peaks in a ROOT script that is in C++. The script can be written to prepare an output of certain peaks existence in binary format. However, optimum sigma (for Gauss distribution) and threshold values have to be determined.

2.5. IDENTIFICATION

Training and target data can be prepared manually for identification analysis. Binary format representing the existence of 5 elements ease the analysis because identification involves existence or absence of an element. Data processing is needed to convert experimental spectra into a format that is similar to training data. This step can be handled by ROOT.

2.5.1. Data Preparation. To represent combination of 5 elements, only 32 cases exists in binary form. Br can be represented by six peaks in gamma spectra, even though there are more. The peaks other than the six peaks have very low intensity in gamma spectra. In order to avoid misidentification, the low intensity peaks were ignored. Similarly, sodium can be represented four peaks (two gamma peaks, two escape peaks from the highest energy). Zinc, potassium, and gold have single peaks with high intensity. These single peaks have an energy lower than 1.022 MeV . Thus, there is not associated single and double escape peaks. In total, 5 elements can be determined by 13 peaks in gamma spectra. Table 2.2 shows a portion of 32 sets of 13-dimensional vector which is prepared manually. Ones represents if there were associated peaks.

A combination of 5 elements is represented by 5-dimensional vector with binary values. One is used if an element exist in the combination and zero if not. Table 2.3 shows a corresponding portion of training data to target data.

2.5.2. Data Analysis. ROOT TSpectrum were used to search peaks and store their information into a text file. In order to find out optimum values for sigma and threshold in the search algorithm, extreme cases such as too low concentration, too low peak counts, too much and too little Gaussian energy broadening in peak shapes can be considered. For low concentrations and low peak counts cases, CINDER'90 was employed. As a consecutive simulation, F8 tally could give the detector response that is similar what was expected from a real detector. The source definition for F8 tally simulation was obtained from CINDER'90 tabulated outputs. For Gaussian broadening, variety of FWHM values were tested. Shift

Table 2.2. A portion of training data

Br	0	0	1	1
	0	0	1	1
	0	0	1	1
	0	0	1	1
	0	0	1	1
	0	0	1	1
Na	1	1	0	0
	1	1	0	0
	1	1	0	0
	1	1	0	0
Zn	1	1	0	0
K	1	1	0	0
Au	0	1	0	1

and gain settings also should be a concern in order to take environmental effects on detector behavior into account. Defining maximum shift and gain setting is crucial for peak scoring in the peak search. Rather than looking at a certain energy for a peak, it is more convenient to look at a range of energy for a peak to cover changes in shift and gain settings of detectors.

2.5.3. Perceptron Network. Linear perceptron network was employed to identify five elements from gamma spectra. Preliminary work turned out that optimization for the network was not needed. Thus, the default perceptron learning and hard limit transfer function were used in the identification step. The input layer of the network consists of 13 neurons for 13 peaks while the output layer has 5 neurons for 5 elements. As hardlimit function is suggested for binary classification [29], it is used as the transfer function to result in zeros and ones in the output. The reason that outputs are either zeros or ones is the hardlimit function.

Table 2.3. Corresponding portion of target data.

Br	0	0	1	1
Na	1	1	0	0
Zn	1	1	0	0
K	1	1	0	0
Au	0	1	0	1

2.6. QUANTIFICATION

2.6.1. Experimental Data. Samples were irradiated under 100 kW reactor power at Missouri University of Science and Technology Reactor (MSTR). MSTR is a test reactor with a limitation of 200 kW as maximum power. It has an open pool type moderator. Neutron flux was

- Thermal neutrons $flux = 2.15 \times 10^{12} ns^{-1} cm^{-2}$ 100 kW
- Epithermal neutron $flux = 2.39 \times 10^{10} ns^{-1} cm^{-2}$ 100 kW

at the time of experiments.

The samples were prepared in powder form to reduce self-shielding and dried to avoid humid pick-up. Prepared samples were irradiated for 3 hours. They were allowed to decay and measured for different time periods. However, the best condition to detect the trace elements was obtained when irradiated samples were let to decay for 96 hours and measured for 8 hours. Delayed gamma was obtained by a high purity germanium (HPGe) detector (Canberra BE3825). Prospect software stored the gamma spectra from the detector in 16,384 channels and energy of range $E \leq 3MeV$. For test and validation purposes, 5 mg NaCl sample with known impurities was irradiated under the same experimental setup. Figure 2.3 outlines the experimental setup.

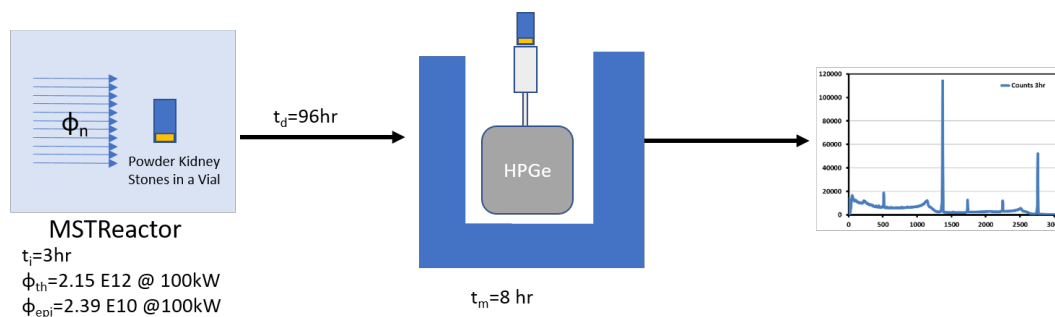


Figure 2.3. Experimental setup for kidney stone samples.

2.6.2. Simulated Data. Monte Carlo simulation can generate required data set for neutron activation of five elements. Number of particles emitted after irradiation can be scored by F1 tally. After simulating variety concentrations of five elements, counts at certain energies can be extracted. Selection of five peaks with the most count is adequate to represent five elements. However, stored counts are the counts from perfect system. A perfect system in MC simulations means 100% detector efficiency, no contamination, and no impurities. Real detectors where impurities, contamination, and 20-40% efficiencies are associated with, would result less counts from an irradiated sample compared with MC simulations. Therefore, energy dependent correction for five peaks are needed. This correction can be made with standard samples that are irradiated under the same experimental conditions as unknown samples.

2.6.3. Neural Network. Three layers including input layer, hidden layer, and output layer were used in quantitative analysis. To find out better structure of the neural network, the number of neurons in the hidden layer were analyzed for three the most used algorithms. When one algorithm which responded better or in acceptable error range was selected, different sizes of training data were analyzed. Based on the result, the ideal size of the training data could save time in a data preparation.

Simulated delayed gamma lines with F1 tally results were collected to obtain 260 sets of data. Then, for the quantification purpose 5 peaks with the most count from 5 elements were extracted from 1024 bins of energy. This process is called feature extraction. Rather than introducing 1024 bins to the data set, 5 peak counts were used to represent 5 elements in the neural network. One spectrum out of 260 spectra were left out in the analysis to evaluate the neural network externally. Finally, training data input consisted of 259 sets of 5-dimensional vector. Figure 2.4 is a representation for the network with 23 neurons in the hidden layer. In the structure, hyperbolic tangent sigmoid function was shown for the hidden layer and linear function for the output layer. In order to avoid zeros for zero outputs for zero or very small inputs, bias was used in the layers as an additional weight.

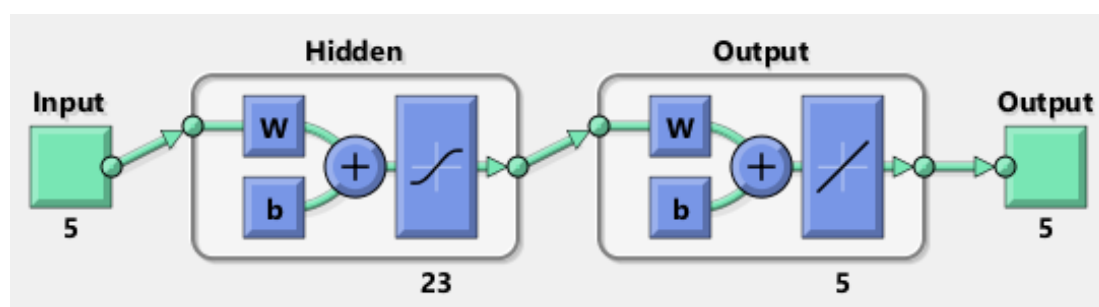


Figure 2.4. Three-layer Neural Network with 23 neurons in the hidden layer

The target contained masses of 5 elements that resulted in 5 neurons in the output layer. The number of neurons in the hidden layer were chosen from 1 to 100 for three LM, BR, SCG algorithms. The training data size also was analyzed for better results in training algorithm. During training, the neural network analyzes the relation between input and known output. Once the relationship (neuron connection weights) is found out, then, the network can analyze input which is unknown to the network. Evaluation of an output from the neural network result gives information about the quality of the network externally. The quality of the network could be also analyzed by performance of the learning stage by looking at performance index behavior. The performance index can be MSE, sum squared error (SSE), sum absolute error (SAE), cross-entropy performance, etc.

Identification and quantification analysis of a sample could be done in a sequential manner. First, a network analyzes whether 5 elements were present in the sample or not. Then, analyzed elements peak values extracted from the spectrum. Peak values were corrected with correction parameters obtained earlier. The new values were used as input to the other network that was trained for quantification. The results gave the total neutron activation analysis of 5 elements in the end. Although 5 elements were used in this study, it was not a limitation. More intensive and larger preparation could result in a sequential neural network analysis of neutron activation up to $Z \leq 92$ elements. This would require very long time. Nevertheless, the advantage would be that the requirement is only for one time preparation. This approach to generalize the analysis to variety decay time would require classification of short half-life, medium half-life, and long half-life. If a neutron activation of a sample requested, then three samples out of one given sample could be prepared for three different experimental setups to observe short, medium, long half-life.

3. RESULTS

Monte Carlo simulation with F1 tally resulted line distribution in a spectrum. Figure 3.1 shows delayed gamma spectrum with 8 hour counting after 3 hour irradiation and 96 hour decay time. After neutron capture by salt (NaCl) sample, Cl which has two naturally occurring isotopes produced two radioisotopes. ^{36}Cl has 3×10^5 year half-life and no known gamma emission while ^{38}Cl has short half-life (37 min) with 4 known gamma emissions. ^{38}Cl radioisotope did not survive for the experimental setup that was simulated. Therefore, only ^{24}Na gamma emission was visible in the spectrum. Contaminating elements on NaCl sample were not enough to produce peaks in the spectrum.

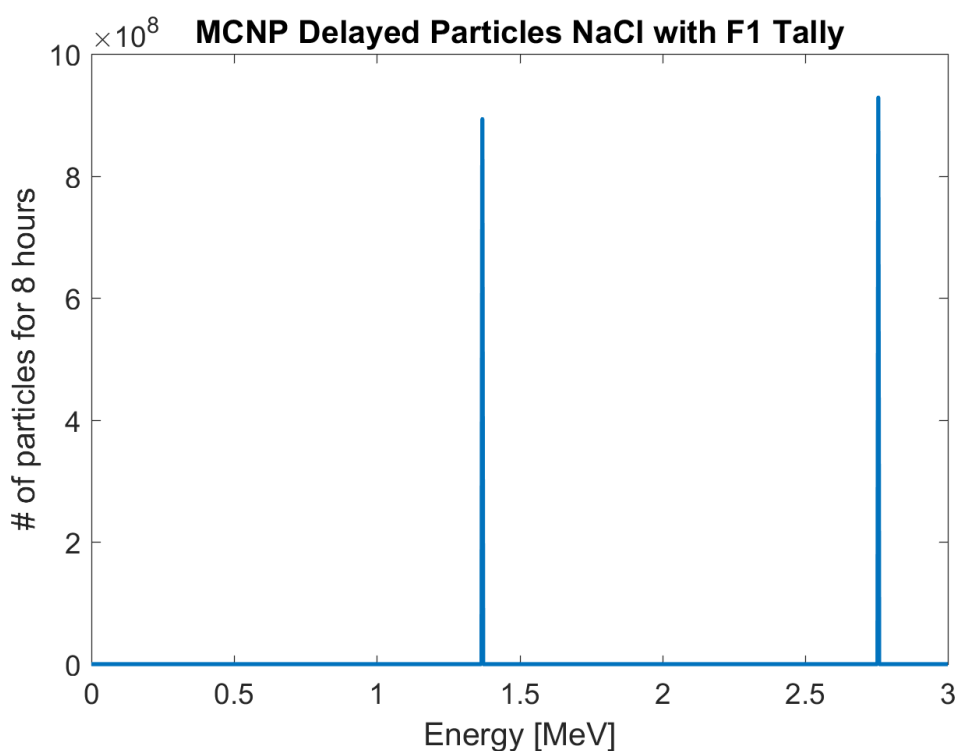


Figure 3.1. MCNP F1 tally simulation of delayed gammas from NaCl sample

F1 tally did not represent the detector response. Nonetheless, it resulted only number of particles emitted in the 8 hour decay time. Two peaks from ^{24}Na that has emission with 100 and 99.9% intensity were shown in the spectrum equally. In real detector measurement, due to single escape peaks, double escape peaks, two peaks did not have the same height. The experimental spectrum also had annihilation peak, backscattering peak appeared on a spectrum. As a consequence, F1 tally gives just number of photons coming from an origin.

On the other hand, escape peaks, annihilation peak and Compton Edge became visible when F8 tally was used. Since both peaks from ^{24}Na were greater than 1.022 MeV, escape peaks from the two energies appeared as well as annihilation peak. Figure 3.2 showed the features as a spectrum.

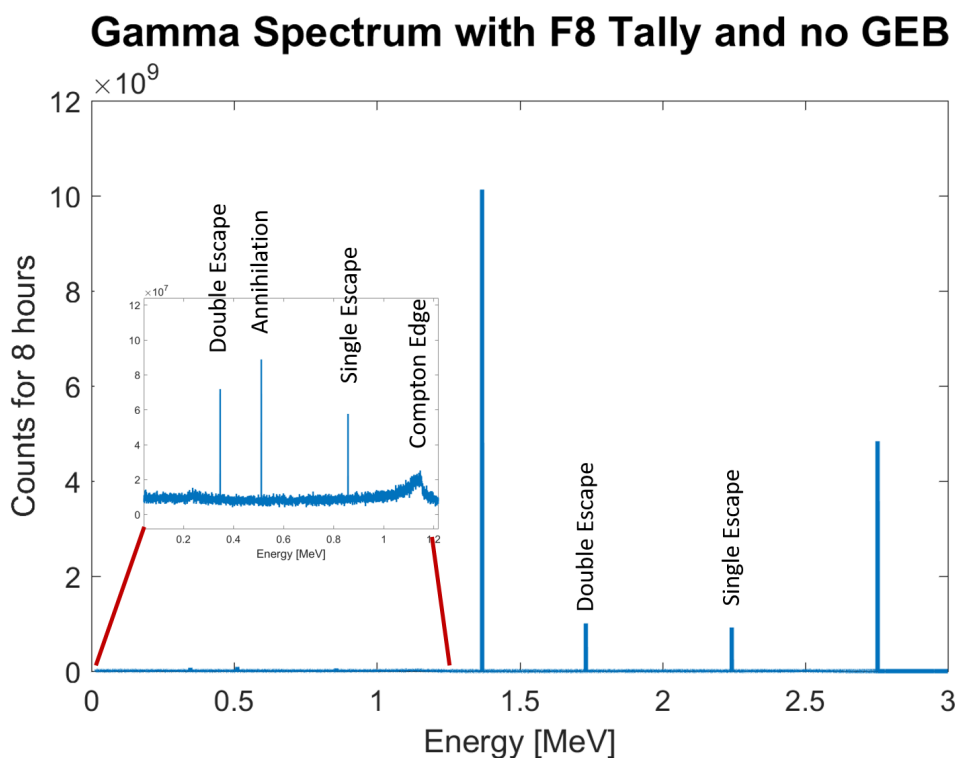


Figure 3.2. MCNP F8 tally simulation of delayed gammas from NaCl sample when no GEB card present.

Yet, this representation was not enough to fully mimic a detector response. Broadening effect on signal had to be taken into account. MCNP simulated the broadening with a special treatment card with a , b , c parameters. To find out a , b , c , parameters in Equation 2.1 in order to use in the GEB card, wide range peaks were analyzed. MATLAB was used to fit the function. Figure 3.3 shows the fitting plot. Table 3.1 represents the parameters with their standard deviations. Although, the standard deviations were found large, especially for c ; simulation resulted suitable broadening in comparison with experimental data. a was the dominant parameter in the equation. Thus, b and c values with large standard deviations did not distorted the peaks much.

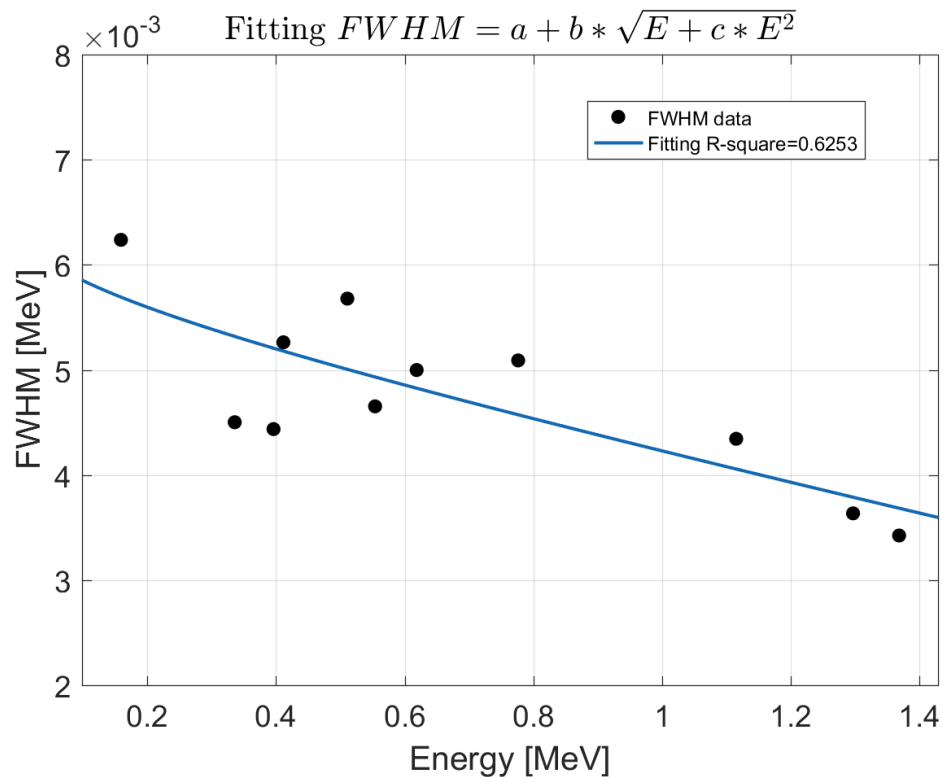


Figure 3.3. FWHM function fitting for the parameters.

Application of GEB parameters resulted in the gamma spectrum in Figure 3.4. In the spectrum, two peaks which had almost same height in F1 tally appeared with different height with F8 tally as they were observed experimentally. The higher energy peak caused

Table 3.1. FWHM parameters for the GEB card in MCNP.

Parameters	Value	StDev
<i>a</i>	0.1204000000	0.0111037201
<i>b</i>	-0.0000598559	0.0000665126
<i>c</i>	-0.0003492000	15.410000000

single and double escape peaks within the detector material. The Compton edge also was visible in the spectrum. After all these steps of MCNP calculation, the simulation setup was ready for mimicking the detector measurements, thus, training data for neural network for identification and quantification.

Both experimental and simulated gamma spectra from APA type kidney stone were compared in Figure 3.5. Except the low energy region, both spectra were in a good agreement. Experimental data had very big noise buildup especially in the X-ray energy range. This was attributed to X-rays from detector and shielding materials as so many gamma rays was emitted.

ROOT estimated the background of the spectra. An example to this background estimation was given in Figure 3.6 from APA type kidney stone. Estimation resulted in a good estimation for The Compton region and high noise region appeared at low energy range. The estimated background was subtracted from the original spectrum to obtain Gaussian peaks only (Figure 3.7). A ROOT code searches the location of 13 peaks representing 5 elements. Then, the code produced a text file by scoring ones if peaks existed in defined energy region and zeros if not.

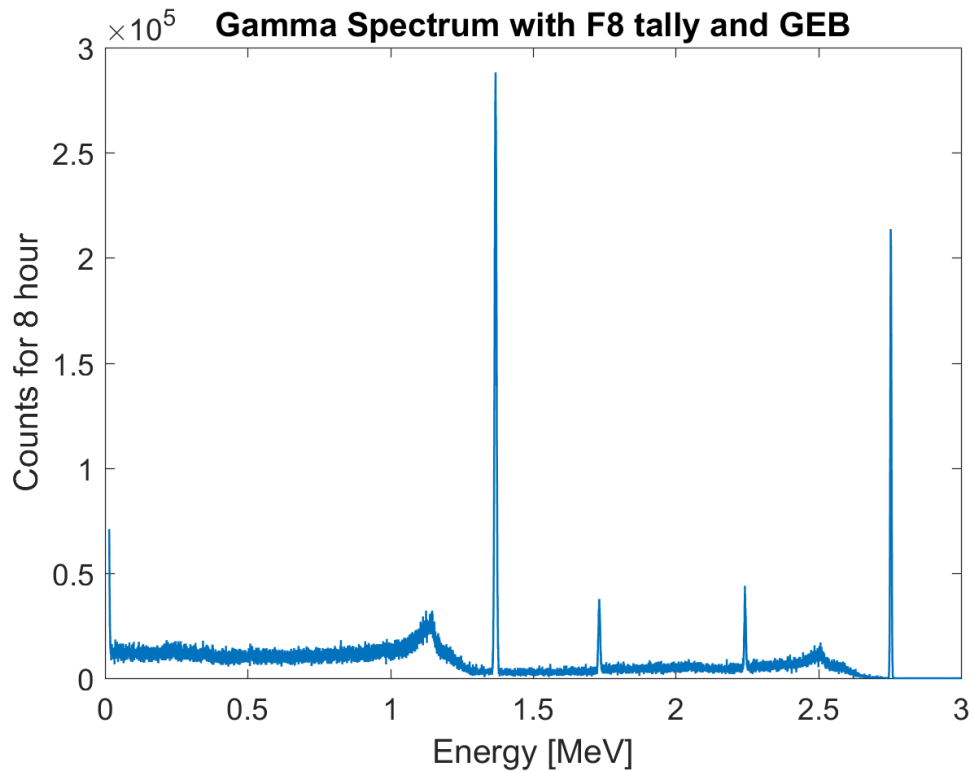


Figure 3.4. MCNP F8 tally simulation of delayed gammas from NaCl sample when GEB card applied.

3.1. IDENTIFICATION

One layer perceptron network was constructed as described in Figure 3.9. Set of 32 vectors with dimension of 13 was used as input to calculate weights in the network by comparing with set of 32 vectors with dimension of 5 for target values. The result of confusion matrix in Figure 3.8 shows that there is a strong linear relationship between training data and target values. The green boxes in the figure outlines the correct linear relation. The red boxes meant mismatch in the training.

ROOT TSpectrum was used to search for peaks in gamma spectra. After real HPGe detector simulation with F8 tally, proper settings for threshold, FWHM (2.355σ), and energy range for a Gaussian peak were determined. Maximum peak number of 25 was

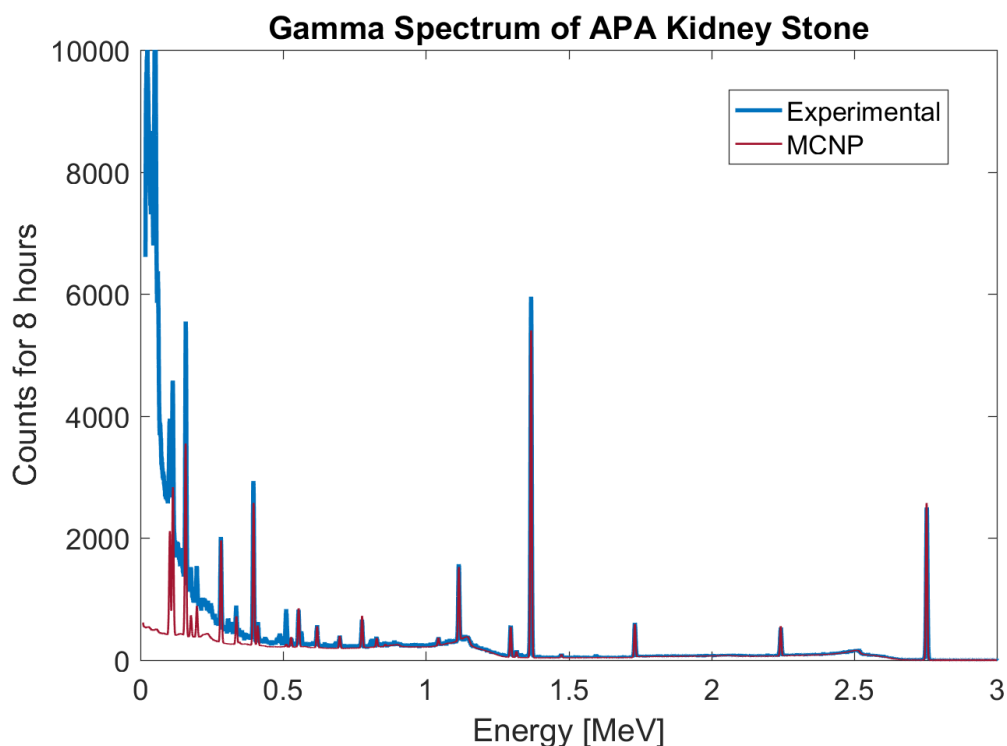


Figure 3.5. Experimental and simulated gamma spectrum from APA kidney stone.

optimum to determine peaks of interest. The intention was to locate 13 peaks. However, maximum peak number was chosen higher because experimental spectra had extra peaks. These peaks were annihilation peak, peaks from other isotopes that were not trace elements signature, and escape peaks from latter.

The settings were able to search for 13 peaks representing five elements. ROOT was used to store the peaks if they were found. It also created an output as a text file with ones and zeros with additional ROOT coding. Ones represented if peaks existed in the energy range, and zeros represented no peak. In addition, various cases were simulated with CINDER'90 and MCNP F8 tally. Example MCNP and CINDER'90 files were given in the Appendices. Every possible combination for five elements resulted in 32 cases with

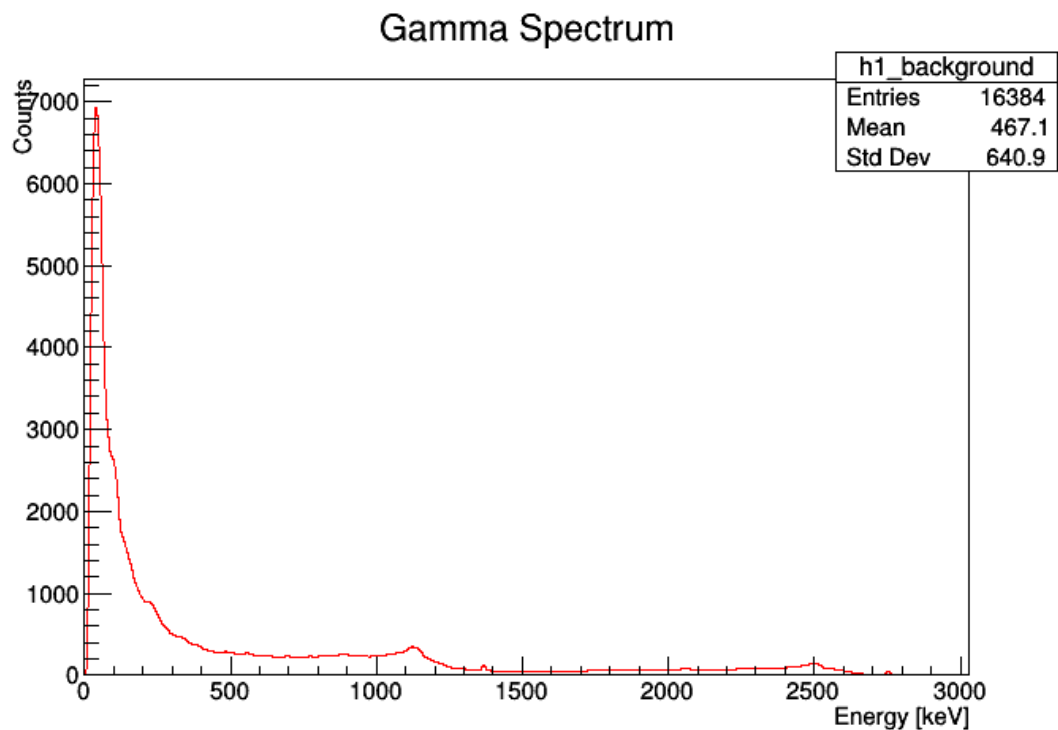


Figure 3.6. ROOT analysis of the APA spectrum for background.

zero combination that does not have to be simulated. In the end, the training data would consist 32 sets of 13 dimensional vector in binary form. The target included binary form of 32 sets with 4 digits.

The binary training data and target data was used in training linear perceptron classification. Figure 3.9 shows linear perceptron structure with 13 dimensional input and 5 dimensional output vector.

Example of identification was made with the experimental data. Gamma spectra from kidney stone samples were used. Table 3.2 summarizes the results for experimental analysis. Analysis failed only testing Au in 8 hour spectrum. This was due to less counts for Au in the spectrum. Although the spectrum analysis with ROOT failed storing two peaks

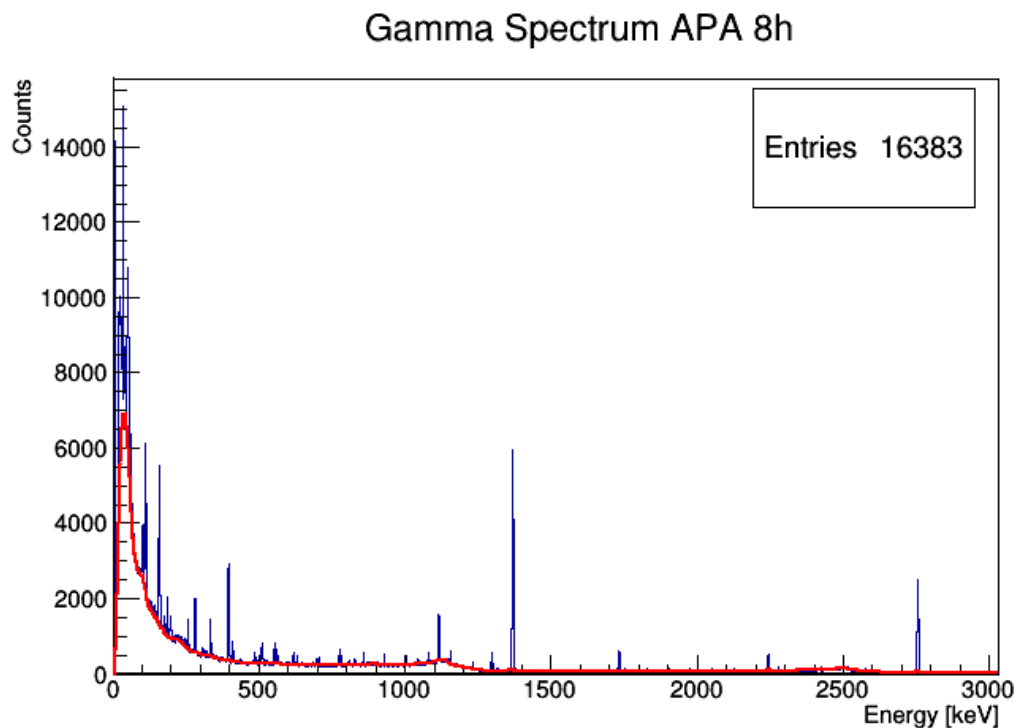


Figure 3.7. Background subtraction from the spectrum.

from Br, storing other four peaks from Br was still recognized by perceptron network. The network resulted correct analysis. If the false reading from a spectrum for a single gamma emitting radioisotope happened, the network would result a false analysis.

3.2. QUANTIFICATION

Simulated data was prepared by using F1 tally to irradiate a sample. The direct use of F8 tally resulted in erroneous spectra or spectra that were not exact representation of detectors. Exact scenario of neutron activation has two step processes. First, the samples are irradiated. Second, irradiated samples are moved to detectors to acquire gamma spectra. The same procedure was meant to be followed by simulating F1 tally responses with time information. The emitted particles after irradiation could be stored to use in the second simulation with F8 tally to mimic the same response as detectors. However, SSW card

Training Confusion Matrix

Output Class	1	17 53.1%	0 0.0%	0 0.0%	0 0.0%	0 0.0%	100% 0.0%
	2	0 0.0%	8 25.0%	0 0.0%	0 0.0%	0 0.0%	100% 0.0%
	3	0 0.0%	0 0.0%	4 12.5%	0 0.0%	0 0.0%	100% 0.0%
	4	0 0.0%	0 0.0%	0 0.0%	2 6.3%	0 0.0%	100% 0.0%
	5	0 0.0%	0 0.0%	0 0.0%	0 0.0%	1 3.1%	100% 0.0%
			100% 0.0%	100% 0.0%	100% 0.0%	100% 0.0%	100% 0.0%
		1	2	3	4	5	
		Target Class					

Figure 3.8. Confusion matrix for linear perceptron.

used in the first simulation stored every particle including prompt gamma as well as delayed gamma emissions. It was not enabling users to store only desired particles. As a result of the fact that F1 tally results were compared with simulated data. And peak information was used instead of whole spectrum in the neural network.

A starting point to find better training algorithm was comparing three algorithms with varying the number of neurons in the hidden layer. Figures 3.10, 3.11, 3.12 show the relative error for 5 elements. In Nuclear Engineering discipline, the results of neutron activation analysis are reported as values and associated relative error. Thus, results were interpreted according to relative error. Number of neurons in the hidden layer from 1 through 100 were simulated. Data was divided into three sections randomly as 70% for

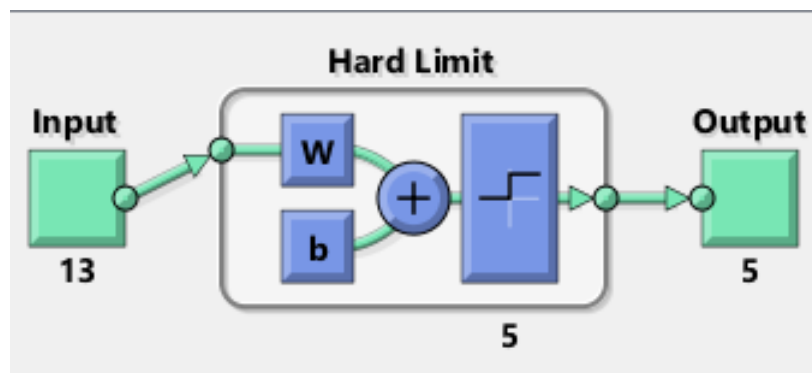


Figure 3.9. Construction for perceptron network representation.

training, 15% for test, 15% for validation. Mean squared error was used as performance function during all neural network simulations. Maximum number of validation fails, μ , and maximum gradient were used as default values offered by MATLAB.

LM algorithm resulted stable relative error distribution (Figure 3.10). The lowest relative error for all elements was with 23 neurons in the hidden layer. Zn was resulting the highest error almost for all hidden layer sizes. This was attributed to decay half-life of Zn. Half-life of Zn is relatively higher than all other elements. Decay of Zn produced small number of gamma emission for different Zn concentration. Therefore, the neural network did not gain enough sensitivity to catch a change in the amount of Zn. The simulation of varying sizes of the hidden layer took shorter time with LM algorithm.

BR algorithm resulted higher relative error shown in Figure 3.11. Even though lower relative error than LM algorithm appeared in between 10 to 15 neurons range in the hidden layer, the error distribution was not stable. After several trials, large changes in the error was observed. In other words, the optimum neuron numbers are different at every run. BR algorithm took relatively longer time than LM algorithm. If size of training data was very large, BR results were expected to be similar to those from LM algorithm. The probabilistic approach was expected to result the same as numeric approach. This is due to the nature of the algorithms. LM was numeric approach to find correct weights whereas BR

Table 3.2. APA type kidney stone test for identification

Elements	3 hour spectrum		8 hour spectrum		12 hour spectrum	
	Estimated	Present	Estimated	Present	Estimated	Present
Br	1	1	1	1	0	0
Na	1	1	1	1	0	0
K	1	1	0	0	0	0
Zn	0	0	1	1	1	1
Au	0	0	0	1	0	0

was probabilistic approach. Main advantage of BR was memory requirement was small. However, it took more time. LM was preferred over BR with confidence because overfitting was not a concern.

SCG which is used mostly in pattern recognitions resulted in very high relative errors. The error distribution was unstable with an increasing trend as the number of neurons in the hidden layer was increased. Figure 3.12 shows the unstable nature of the error distribution based on neuron numbers. The results were noted as suspicious. SCG did not take time as much as BR; but, it took longer than LM algorithm.

Comparison of three algorithms with different size of hidden layers suggested to use LM algorithm with 23 neurons in the hidden layer.

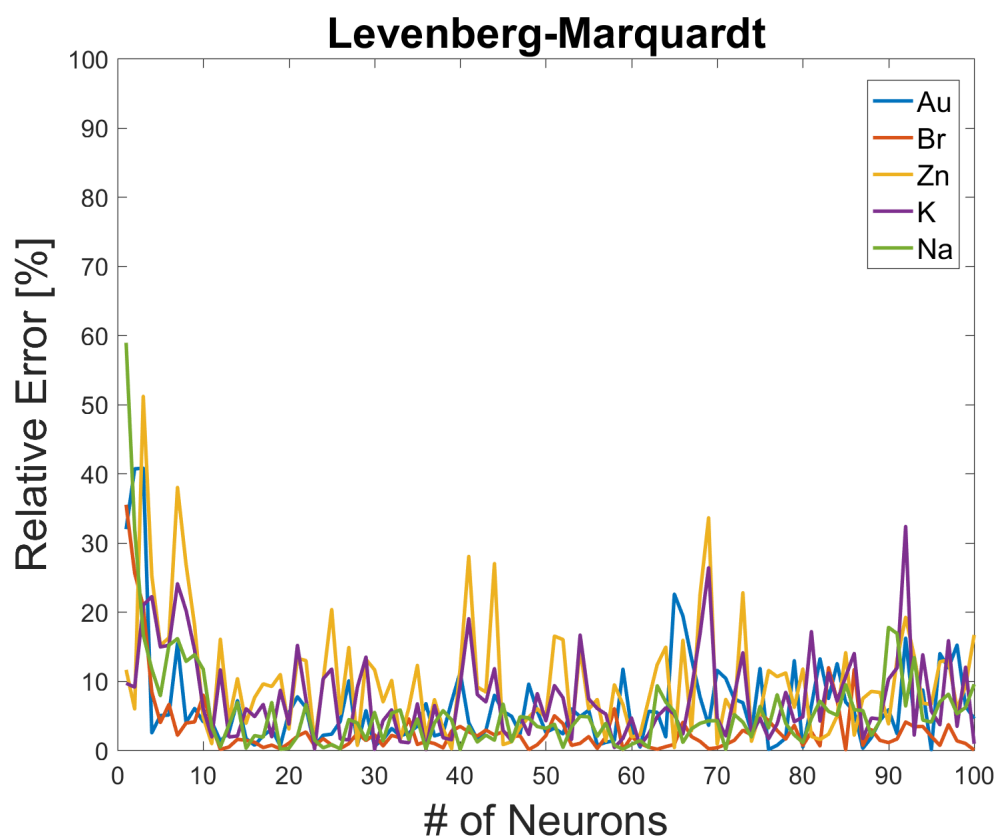


Figure 3.10. LM error with different number of neurons in the hidden layer.

Next step was to observe the response dependency of the network based on the size of the training data. LM algorithm was used with 23 neurons in the hidden layer to test training data size. Figure 3.13 shows the result of different training data sizes.

The average relative error of 5 elements would introduce bias to the evaluation because a very high and a very low error might result an acceptable error when averaged. Thus, highest relative error from 5 elements was stored and plotted to validate the training data size. Figure 3.13 suggested that 220 set of input vectors were required if the goal was less than 10% relative error. Since 259 set of input vectors were available, the study was carried using all the data set.

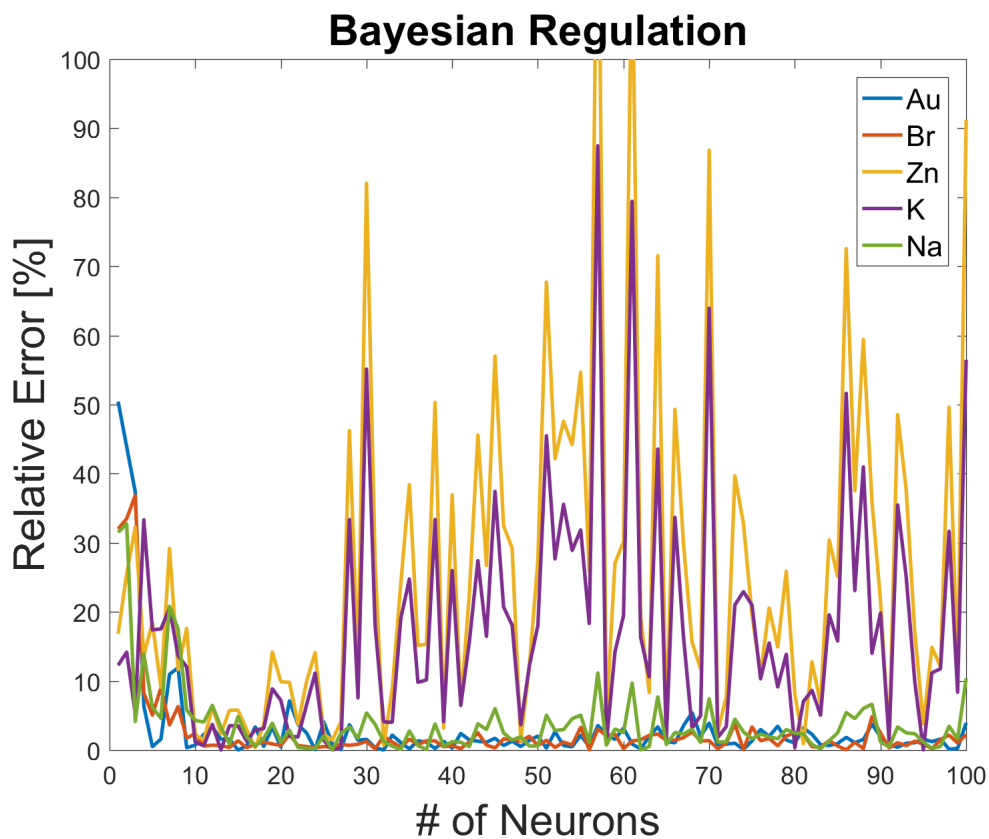


Figure 3.11. BR error with different number of neurons in the hidden layer.

Finally, LM algorithm was used with 259 sets of 5-dimensional input vectors and 23 neurons in the hidden layer. Figure 3.14 represented high correlation ($R=0.99669$) between input and output of the network for all cases. The figure also showed that random generations of concentration of five elements were highly homogeneous. The dashed line stood for perfect results. The solid green line represented fitted results. Because of the high correlation, fitted line and dashed line overlapped.

Training data due to random selection had high correlation between target and the neural network output. High concentration values were observed to serve quality response even though less data was observed in the region. The correlation value ($R = 0.99759$) was higher than for all cases together. The distribution was shown in Figure 3.15.

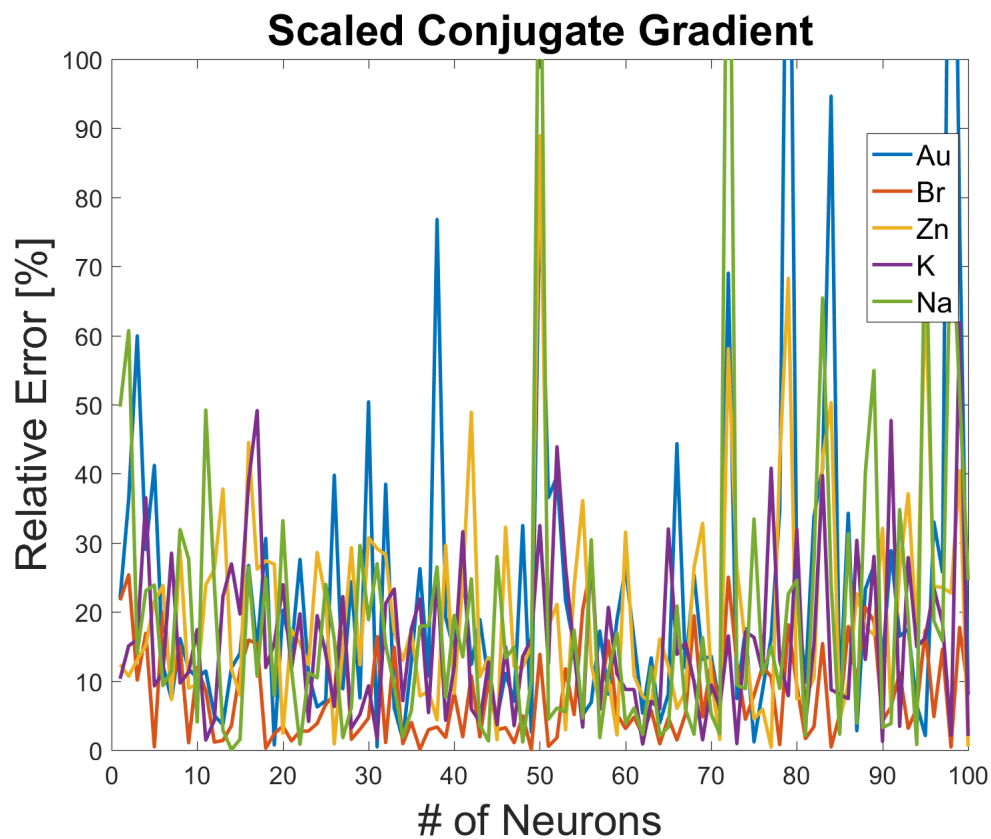


Figure 3.12. SCG error with different number of neurons in the hidden layer.

Figure 3.17 and Figure 3.16 also showed high correlation in fitting. The validation and test processes had almost homogeneous random choice. The circles were distributed along the fitted line (green line). This choice was different for every run as data separation for training, validation, and test was randomly selected. The distribution could be selected to provide more homogeneous distribution. However, the accuracy was at desired level such that further improvement was not required.

The target that consisted of concentration of 5 elements were divided by mass of the sample in the simulation. As a result, the unit of target was element concentration per unit mass.

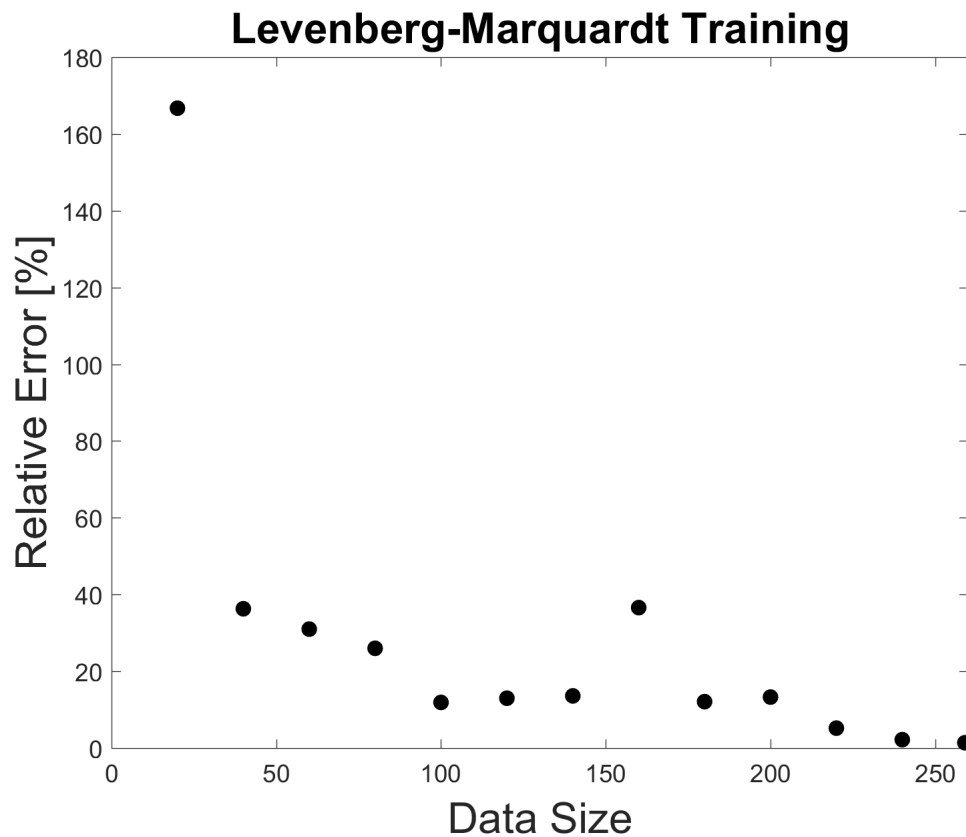


Figure 3.13. LM error with different size of training data.

Mean squared error (MSE) was used for the performance. When validation started to fail the training was stopped by LM algorithm. The behavior is shown in Figure 3.18. The validation was stopped when MSE was found as minimum. The validation was carried on for six more iteration to ensure the error was not getting any better. The test curve (red line) did not show any increase before the validation curve (green line) in the figure. Thus, it was confirmed that there was no overfitting problem occurred in the training step. By analyzing the regression fitting and the MSE plot, it was concluded that random choice of 70% training data, 15% validation data, 15% test data was a suitable configuration for the data. MSE performance function resulted in better training compared with other type of performance functions.

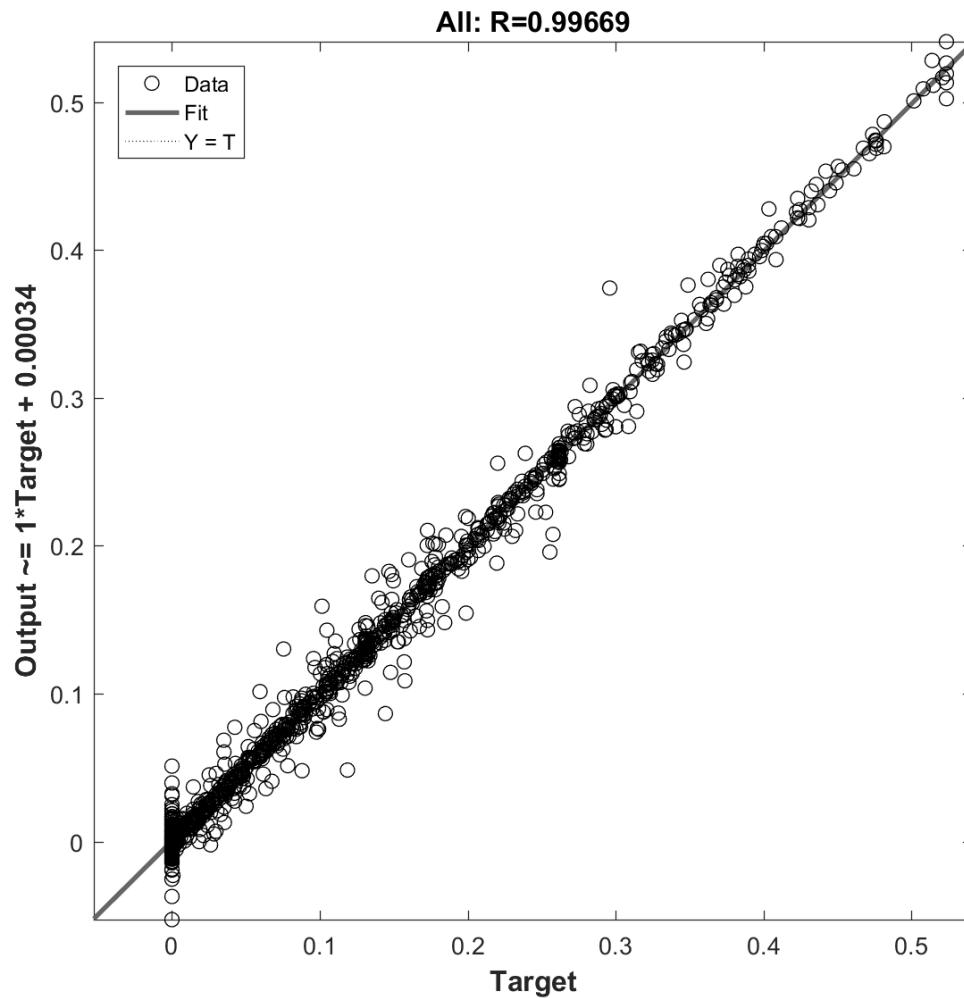


Figure 3.14. Regression plot for training, validation, and test.

The output of the network was giving both positive and negative values. Because the mass concentration values should be between 0 to 1, logarithmic sigmoid (logsig) function was used to constrain the output to [0,1] range. However, this constrain forced the network to end up with bad MSE during training. The hyperbolic tangent sigmoid (tansig) function was also used as well. As the tansig function resulted in almost same response, the default option for the output layer was taken as purelin transfer function.

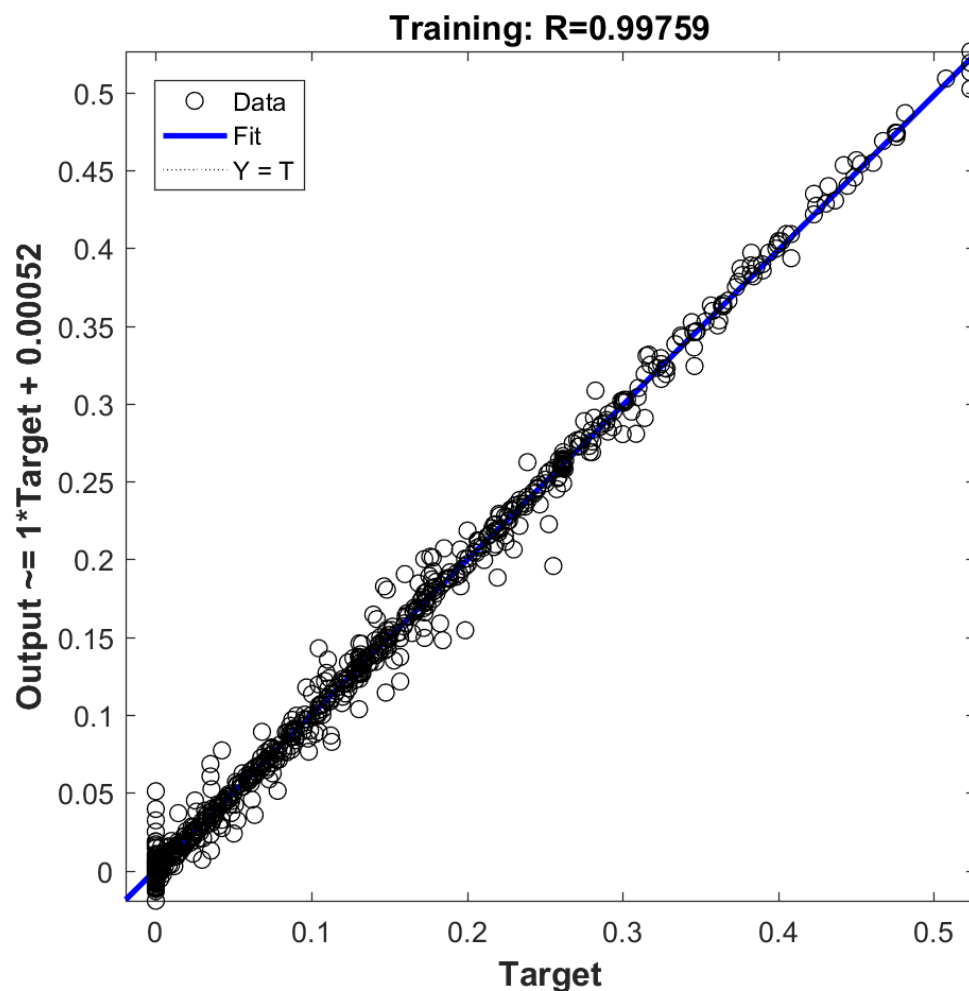


Figure 3.15. Regression plot for training.

Table 3.3 is a summary of external validation for the NN with 5-23-5 (5 neurons in the input layer, 23 neurons in the hidden layer, 5 neurons in the output layer). According to the results, the highest error was obtained as 5.4% from Zn. This was previously attributed to the longer half-life of Zn in the simulation. Less decay in the simulation produced less particle that the network during training loses its sensitivity to Zn to some extent. Nonetheless, the tabulated values are still in high precision when compared with the literature that have reported results from simulation only.

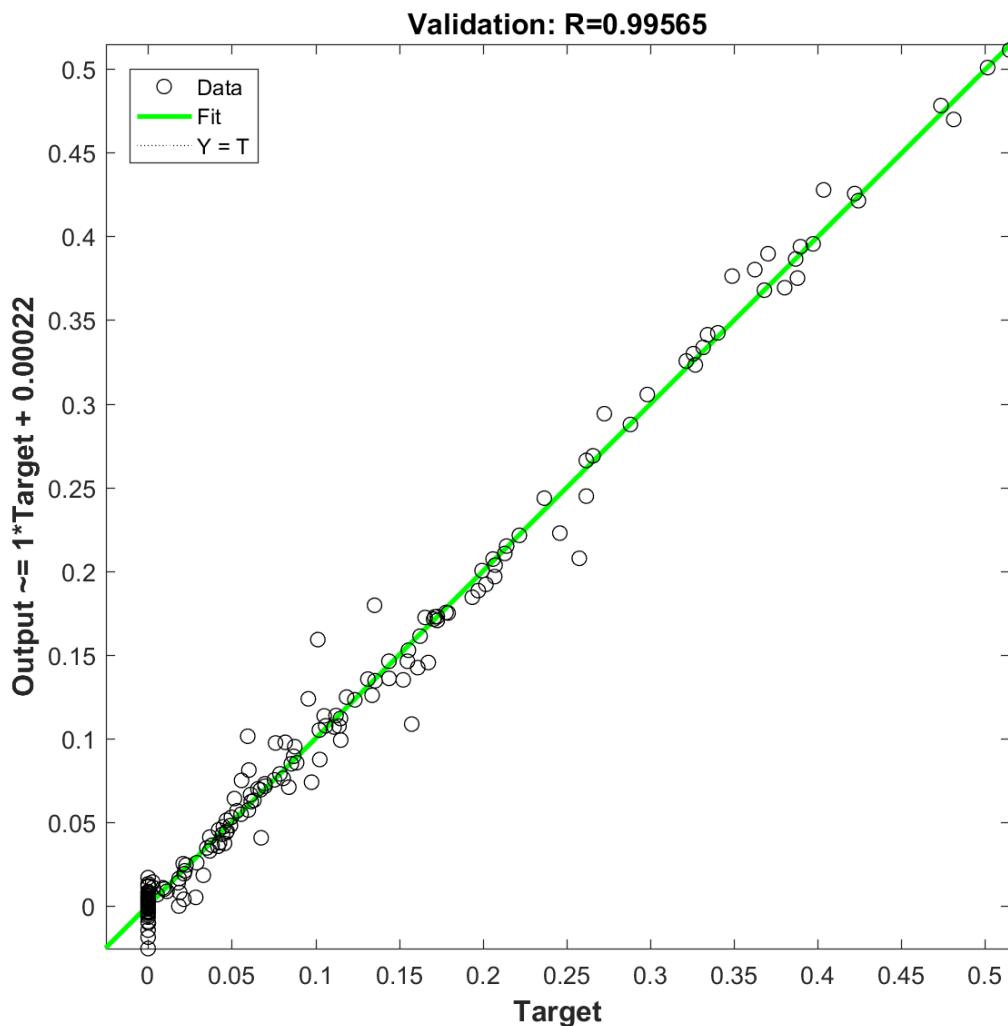


Figure 3.16. Regression plot for validation.

Table 3.4 shows the relative error on the analysis of kidney stone spectra with the neural network. As it was expected, there were high relative error associated with Zn. Some errors were above 10%. This was attributed to the correction between simulated spectrum and experimental spectrum. Although large error occurred, simulated analysis results in Table 3.3 says that if better correction was obtained between simulated spectra and experimental spectra, the error can be as low as 5.4%.

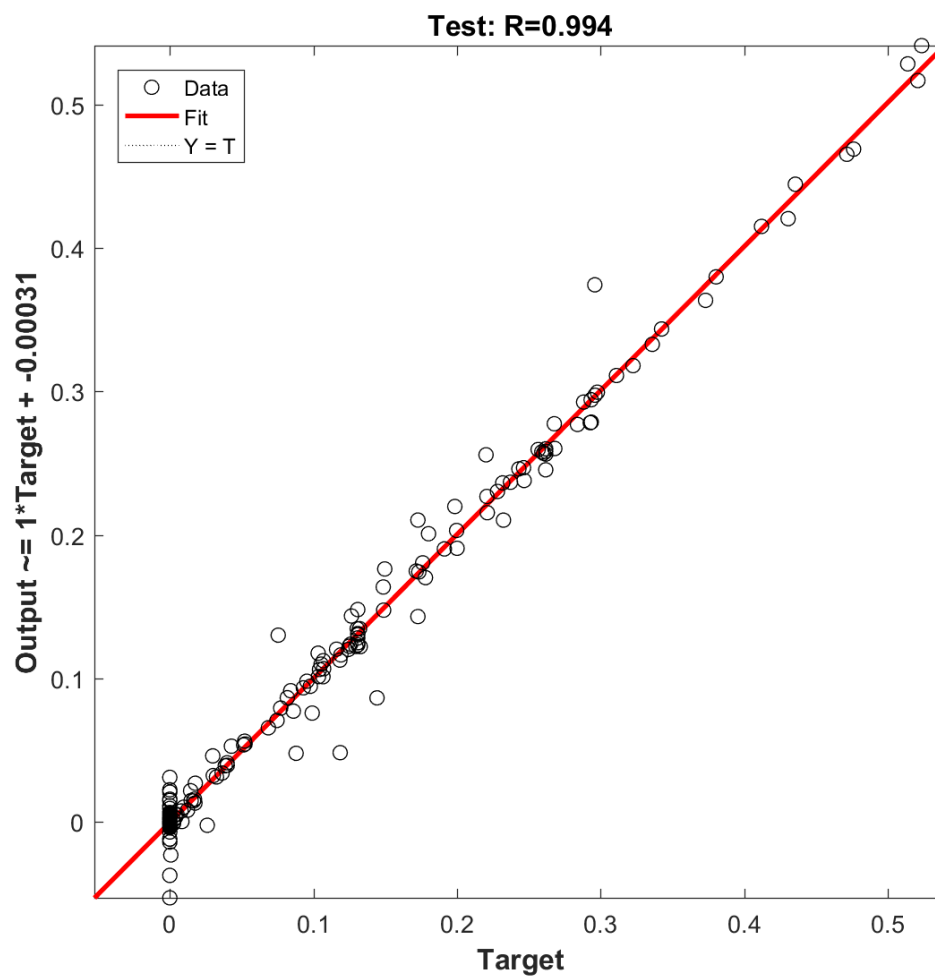


Figure 3.17. Regression plot for test.

Artificial neural network was successfully applied to neutron activation analysis. Increase in number of element for analysis requires larger training data for future studies. However, five elements were enough to perform activation analysis for bio-samples for the purpose stated earlier. Overall, the neural network parameters and functions for accurate analysis of trace elements in gamma spectra were summarized in Table 3.5 in detail.

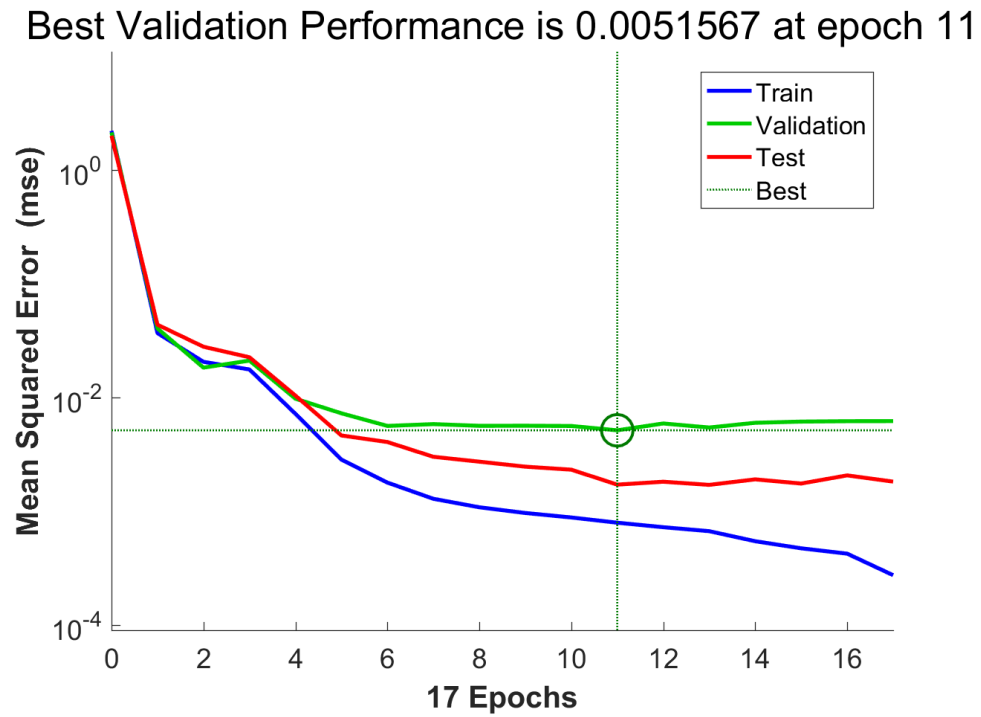


Figure 3.18. MSE values during training with purelin function in the output layer.

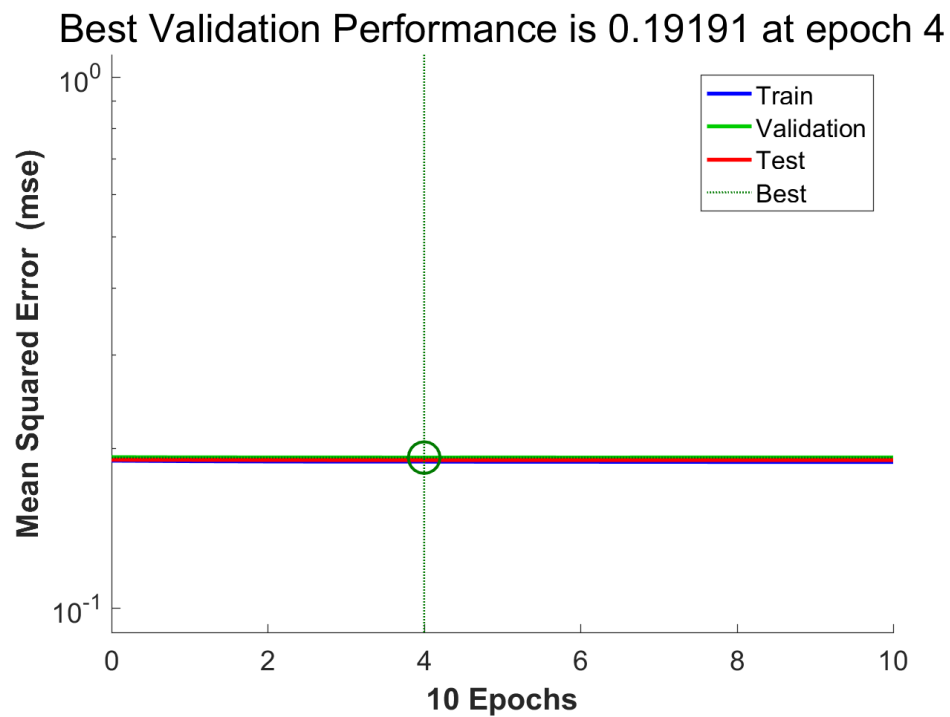


Figure 3.19. MSE values during training with logsig function in the output layer

Table 3.3. External validation of the neural network.

Elements	Concentration	NN result	Relative error %
Br	0.066025834	0.0648	1.8
Na	0.171845192	0.1661	3.4
Zn	0.091106226	0.0960	5.4
K	0.122679246	0.1261	2.8
Au	0.071942503	0.0708	1.6

Table 3.4. Neural network analysis of experimental spectra for relative error in %.

Elements	APA	COM	UA	STRU
Br	5.3	10.1	16.0	14.6
Na	7.2	12.3	8.7	9.0
Zn	17.9	28.2	24.9	27.9
K	N/A	N/A	21.1	N/A
Au	5.2	9.9	5.4	16.1

Table 3.5. Summary of the optimum neural network.

Features	Assigned Value
Train function:	Levenberg-Marquardt
Number of layers:	3 (input-hidden-output)
Number of neurons in the hidden layer:	23
Number of neurons in the input layer:	5
Number of neurons in the output layer:	5
Devide mode:	Random
Performance function:	MSE
Bias connections:	[1;1]
Maximum number of Epochs:	1000
Maximum number of fails:	6
μ :	[0.001 – 1e10]

4. CONCLUSIONS

Artificial neural network has been successfully implemented to the analysis of gamma spectra for qualitative and quantitative analysis. The biggest advantage of neural network is that it takes time only

Monte Carlo simulation was successfully used to generated gamma peak information from neutron capture reactions of irradiated samples. 5 elements which were common in kidney stones were the research focus. Randomly generated mass concentration of these 5 elements were prepared in order to use in the material card of MCNP. Concentrations were normalized to mass of samples that resulting unit was g/g per unit mass. CINDER'90 code was used to simulate radioactive isotopes under the experimental setup. CINDER'90 working with MCNPX generates radioisotope densities over time. The densities were used in further simulations.

Current (F1) tally and Pulse Height (F8) tally were employed to prepare data. F1 tally generates how many particles were emitted during detection time. There was significant difference between detected particles and emitted particles due to detector area, dead time, detector efficiency, etc. Therefore, an energy dependent correction was made for the counts from experimental data. The energy depended corrections for 5 elements were obtained by comparing known samples with their masses and simulated values. 5 peaks were chosen to represent 5 elements. Some of the elements emit gamma particles with more than one energy. In such a case, only the peaks with most count were taken into account. Simulated data was stored to use in quantification analysis in the neural network.

Decay densities tabulated by CINDER'90 were used in F8 tally to mimic gamma spectra from a detector. Application of GEB function with different parameters produced spectra for different detector responses. Different gain and shift settings were applied to obtain different voltage and temperature effects on the spectra.

Several scenarios with different gain and broadening settings were conducted and analyzed with ROOT. Peak search specifics were obtained to search for peaks from experimental gamma spectra with Canberra HPGe detector. Main specifics were sigma of a Gaussian peak, threshold to separate signal from noise, and maximum peak number to search.

Linear perceptron was successfully employed for identification purpose. To train the perceptron network, occurrences of five elements were prepared in binary representation. Then optimized ROOT search algorithm with TSpectrum was used to search for desired peaks. ROOT also was capable of generating a text file in a required format. Output file was generated as in binary format by ROOT. When ROOT found desired peaks, it stored ones to represent the presence of peaks. It stored zeros if desired peaks were not found in a spectrum.

Three layer neural network was employed for quantification analysis. Levenberg-Marquardt algorithm found to be better for the quantification purpose. 23 neurons in the hidden layer was used to get low relative error. 259 set of 5-dimensional vectors were used for training purpose. 5-23-5 Neural Network, trained with LM algorithm, resulted very low error on determination of element concentrations. Maximum relative error was found to be 5.4%. The analysis of experimental spectra resulted error in-between 5.2% and 28.2%. The error was attributed to accuracy of correction parameters between simulated data and experimental data. The techniques promised that once the correction parameters found with better accuracy, the error could be as low as 5.4% as in neural network evaluated with simulated data.

Maximum error in quantification was found from Zn. Due to long half-life of Zn, decay during measurement time (8 hours) was not enough to emit as compared to other radioisotopes. Therefore, the neural network was not trained well for changes in Zn concentrations.

Pulse height (F8) tally was not suitable for quantification analysis due to time binning issue with this type of tally. F8 tally cannot be used with time bins directly. It could be coupled with F6 tally. This method did not mimic the detector representation. SSW card cannot be used with time as in F8 tally. In addition, SSW card took more than 3 hours with i7-quad-core-16GB memory pc for only one single simulation. Consecutive simulations would take more time that was not effective. Besides the summarized limitations, main limitation of data preparation for neural network application was data library of MCNP to produced delayed particles from irradiated samples.

During mass concentration preparation for MCNP material card, the concentration of elements that had low interaction rates or long half-life can be focused to prepare more variety of them. High variation rather than small changes will improve the sensitivity of the neural network for these elements.

In NAA, preparation of training data with Monte Carlo simulation to examine experimental data was the first time approach. Current researchers analyzed simulated data with neural network trained by simulated data. This use is not very practical because simulation represents perfect conditions. However, real life measurements have imperfections. In another use of neural networks, experimental data was used for both training and analysis. This approach also is not found practical because for large training data neutron source as well as detectors should be occupied for long use under the same experimental conditions. Keeping experimental conditions same is almost not possible or so expensive. Temperature, voltage settings, neutron source capability, etc. were some conditions that were not controllable.

In this study, error occurs only in determination of correction parameters between simulated peaks and experimental peaks. Error did not propagate during analysis on the contrary of hand calculations.

Once the neural network was trained, further analysis did not take time while manual calculations would cost the same time during every analysis. Hand calculation with a use of commercial software requires additional feature checking for radioisotopes that emit overlapping energies. That was handled by the trained neural network. The simulated data could also be trained for different experimental setups instead of generating another 260 set of simulated data. This require a careful check on dead time. The experimental data for different experimental conditions should not have significant dead time.

Finally, it is shown that artificial neural network coupled with MCNP was applied successfully on identification and quantification of experimental gamma spectra.

APPENDIX A

NEUTRON ACTIVATION SIMULATION

Thermal neutrons into activation sample

1 1 -1.0 -1 imp:n,p=1

2 2 -0.001205 -2 1 imp:n,p=1

3 0 2 imp:n,p=0

1 so 0.5

2 so 5

mode n p

m1 nlib=.80c

c 35079 0

c 35081 0

11023 -1.0

c 30064 0

c 30066 0

c 30067 0

c 30068 0

c 19039 0

c 19041 0

c 79197 0

m2 7014 -0.756 8016 -0.231 18000 -0.013

act nonfiss=p dg=lines \ \$ Line data

sdef par=n erg=2.53e-8 wgt=2.15e12 tme=d1

si1 H

0e8 10800e8

sp1 0 1

c ssw 1 pty=p

lca 7j -2

f12:p 1

e12 0 1022i 3.0

t12 10800e8 356400e8 385200e8

nps 1000000

c sd11 1

APPENDIX B

PULSE HEIGHT TALLY SIMULATION

PHT from BE HpGe detector

```

c      Created on: Wednesday, November 19, 2014 at 20:52
c 1 1 -1 -1  imp:p=1 $ Kidney stone (water)
2 2 -0.92 -4 -2 3  imp:p=1  $Carbon window
3 3 -2.7 7 -8 -2 (10 :-6 :5 )(10 :-5 :3 )(-10 :5 :9 :-6 )
      (4 :-3 :2 ) imp:p=1
4 4 -5.32 12 -11 -10  imp:p=1 $Ge detector
5 5 -8.96 (-17 15 -13 (10 :-14 :13 )):(-18 19 16 -15 ) imp:p=1
6 6 -0.001205 -20 22 -21 (8 :-7 :2 ) imp:p=1
7 0 -10 14 -12 imp:p=1
8 0 (((6 -9 -5 ):(-10 -3 5 ))(17 :-15 :11 )
(18 :-16 :-19 :14 )):(13 -17 -11 10 ) imp:p=1
9 0 20 :21 :-22 imp:p=0 $outside

```

```

c 1  so 0.5
2  px -3
3  px -3.06
4  cx 3.75
5  px -3.15
6  px -14.7
7  px -15
8  cx 4.45
9  cx 4.3
10 cx 3.5
11 px -3.56
12 px -6.06
13 px -3.71

```

```

14 px -8.86
15 px -9.01
16 px -10.01
17 cx 3.65
18 cx 3.2
19 cx 3.05
20 cx 9.45
21 px 5
22 px -20

mode p e
m2 6000. 1 $carbon window
m3 13000. 1 $Aluminum
m4 32000. 1 $germanium
m5 29000. 1 $cupper for the lateral wall
m6 6000 -0.00039 7000 -0.78081 8000 -0.2095 18000 -0.0093 $air
sdef erg=d1 par=2 pos 0 0 0
# si1 sp1
L D
1.368633 0.357491233
2.754028 0.357291038
1.115546 0.065367718
1.29709 0.031449016
0.776517 0.019747113
0.554348 0.01674366
0.619106 0.010263769
0.698374 0.006737668

```

0.827828	0.005682912
1.044002	0.006439687
1.317473	0.006262318
1.47488	0.003859555
0.396329	0.042859122
0.282522	0.020157181
0.113805	0.012589867
0.158379	0.02042807
0.411	0.006128421
0.197957	0.004085669
0.177214	0.002529006
0.10318	0.008511662
0.33624	0.006833894
0.5279	0.004086937

f8:p,e 4

c e8 0 0.005 16382i 3.0

e8 0 0.005 2046i 3.02

ft8 GEB 0.00670897 -0.0025548 -0.00032

c ft8 GEB 0.00686532 -0.00266048 -0.0004

c ft8 GEB 0.00584912 -5.98559e-5 -0.0003492

c f6:e 4

c f18:p 4

c e18 0 0.0001 0.00056 1019i 3.0

c ft18 phl 1 6 1 0 hpg-1 GEB 5.86828e-4 3.95113e-4 7.46793

nps 1000000000

APPENDIX C

CINDER'90 INPUT

MCNPX CODE FOR IRRADIATION

MSTR irradiation simulation for Neural Network Data

1 2 -1.0 -1 imp:n=1

2 0 -2 1 imp:n=1

3 0 2 imp:n=0

1 so 1.0

2 so 10

mode n

phys:n 25 3j 5

totnu no

print

nps 1000000

sdef erg=d1 pos 0 0 0 par=1 wgt=2.175e12

c ***** MSTR neutron flux *****

si1 H 0 1.0e-6 0.01 20

sp1 D 0 0.9885 0.011 0.0005

c

c m1 6000 -0.00039 7000 -0.78081 8000 -0.2095 18000 -0.0093

m2 nlib=.80c

f4:n 1

e0 5.000e-09 1.000e-08 1.500e-08 2.000e-08 2.500e-08

3.000e-08 3.500e-08 4.200e-08 5.000e-08 5.800e-08 6.700e-08

8.000e-08 1.000e-07 1.520e-07 2.510e-07 4.140e-07 6.830e-07
1.125e-06 1.855e-06 3.059e-06 5.043e-06 8.315e-06 1.371e-05
2.260e-05 3.727e-05 6.144e-05 1.013e-04 1.670e-04 2.754e-04
4.540e-04 7.485e-04 1.234e-03 2.035e-03 2.404e-03 2.840e-03
3.355e-03 5.531e-03 9.119e-03 1.503e-02 1.989e-02 2.554e-02
4.087e-02 6.738e-02 1.111e-01 1.832e-01 3.020e-01 3.887e-01
4.979e-01 0.639279 0.82085 1.10803 1.35335 1.73774 2.2313
2.86505 3.67879 4.96585 6.065 10.00 14.9182 16.9046 20.0 25.0

CINDER'90 CODE FOR ISOTOPE CREATION

title_lines

Irradiation at MSTR for Neural Network

act04 MSTR irradiation

files

bigza_file bigza

mcnpx_outp act04o

cinder_options

tst 1e-5

signif 1e-16

kchn 0

klib 0

nfe 3

nosame 0

russ 1

run_options

dcounter 41

splprods 0

tabular 1

normalization

snorm 1.0

history

1 1.0

3 h

2 0.0

96 h 8 h

cell_list

cell 1

1

APPENDIX D

MATLAB CODE FOR HIDDEN LAYER SIZES


```

% Setup Division of Data for Training, Validation, Testing
net.divideParam.trainRatio=70/100;
net.divideParam.valRatio=15/100;
net.divideParam.testRatio=15/100;

%%%%%%%%%%%%%%%%%%%%%%%%%%%%%%%%%%%%%%%%%%%%%%%%%%%%%%%%%%%%%%%%%%%%%%%%

% Train the Network

[net,tr]=train(net,input,target);

%%%%%%%%%%%%%%%%%%%%%%%%%%%%%%%%%%%%%%%%%%%%%%%%%%%%%%%%%%%%%%%%%%%%%%%%

% Test the Network

y(:,i)=net(spec);
e=gsubtract(target,y(:,i));
performance=perform(net,target,y(:,i));

%%%%%%%%%%%%%%%%%%%%%%%%%%%%%%%%%%%%%%%%%%%%%%%%%%%%%%%%%%%%%%%%%%%%%%%%

% Relative error from expected values
error(:,i)=(abs(conc-y(:,i))./conc);
end

%%%%%%%%%%%%%%%%%%%%%%%%%%%%%%%%%%%%%%%%%%%%%%%%%%%%%%%%%%%%%%%%%%%%%%%%

% Write results to excel files
filename4='nn_results_lm.xlsx';
filename5='nn_errors_lm.xlsx';
xlswrite(filename4,y);
xlswrite(filename5,error);

y; % Uncomment if the output is required to the screen

```

```
error; % Uncomment if the output is required to the screen
```

```
%%%%%%%%%%%%%%%%%%%%%%%%%%%%%%%%%%%%%%%%%%%%%%%%%%%%%%%%%%%%%%%%%%%%%%%% Plots %%%%%%%%%%%%%%%%%%%%%%%%%%%%%%%%%%%%%%%%%%%%%%%%%%%%%%%%%%%%%%%%%%%%%%%%%
```

```
% Uncomment these lines to enable various plots.
```

```
%figure, plotperform(tr)
```

```
%figure, plottrainstate(tr)
```

```
%figure, plotfit(net,x,t)
```

```
%figure, plotregression(t,y)
```

```
%figure, ploterrhist(e)
```

REFERENCES

- [1] S. O. Haykin, *Neural Networks and Learning Machines*. Pearson Education, Nov. 2011.
- [2] M. T. Hagan, H. B. Demuth, M. H. Beale, and O. D. Jesus, *Neural Network Design (2nd Edition)*. Martin Hagan, Sept. 2014.
- [3] A. Srivastava, K. K. Swain, B. Vashisht, P. Aggarwal, U. Mete, R. Acharya, D. N. Wagh, and A. V. R. Reddy, "Studies of kidney stones using INAA, EDXRF and XRD techniques," *Journal of Radioanalytical and Nuclear Chemistry*, vol. 300, pp. 191–194, Apr. 2014.
- [4] S. Sarmani, L. L. Kuan, and M. A. Bakar, "Instrumental neutron activation analysis of kidney stones," *Biological Trace Element Research*, vol. 26-27, pp. 497–502, Dec. 1990.
- [5] V. K. Singh and P. K. Rai, "Kidney stone analysis techniques and the role of major and trace elements on their pathogenesis: a review," *Biophysical Reviews*, vol. 6, pp. 291–310, July 2014.
- [6] K. Hobarth, C. Koeberl, and J. Hofbauer, "Rare-earth elements in urinary calculi," *Urological Research*, vol. 21, no. 4, pp. 261–264, 1993.
- [7] G. V. Iyengar, "Human health and trace element research: problems and prospects," *The Science of the Total Environment*, vol. 19, pp. 105–109, June 1981.
- [8] M. V. Frontasyeva, "Neutron activation analysis in the life sciences," *Physics of Particles and Nuclei*, vol. 42, pp. 332–378, Mar. 2011.

- [9] N. Tsoufanidis, *Measurement and Detection of Radiation, Third Edition*. CRC Press, Nov. 2013.
- [10] <http://nmi3.eu/neutron-research/techniques-for-/chemical-analysis.html>, *The NMI3 information portal*. Accessed: June 2017.
- [11] G. T. Seaborg and J. J. Livingood, "Artificial Radioactivity as a Test for Minute Traces of Elements," *Journal of the American Chemical Society*, vol. 60, pp. 1784–1786, Aug. 1938.
- [12] D. R. Chettle and J. H. Fremlin, "Techniques of in vivo neutron activation analysis," *Physics in Medicine and Biology*, vol. 30, no. 5, p. 478, 1985.
- [13] G. Gilmore, *Practical Gamma-ray Spectroscopy*. John Wiley & Sons, Sept. 2011.
- [14] H. Sahiner, A. Srivastava, C. H. McCollough, and X. Liu, "Neutron activation analysis with a Monte Carlo simulation for kidney stones," *Biomedical Physics & Engineering Express*, vol. 1, no. 4, p. 045103, 2015.
- [15] S. M. Lin, C. L. Tseng, and M. H. Yang, "Determination of major, minor and trace elements in urinary stones by neutron activation analysis," *International Journal of Radiation Applications and Instrumentation. Part A, Applied Radiation and Isotopes*, vol. 38, no. 8, pp. 635–639, 1987.
- [16] G. F. Knoll, *Radiation Detection and Measurement*. New York: John Wiley /& Sons, 3rd ed., 2010.
- [17] G. M. Crankovic, *ASM Handbook: Materials Characterization*, vol. 10 of *ASM Handbook Ser.* Materials Park: ASM International, 9th ed., 1986.
- [18] <https://www.iaea.org/topics/research-reactors>, *International Atomic Agency*. Accessed: June 2017.

- [19] J. E. Turner, *Atoms, Radiation, and Radiation Protection*. John Wiley & Sons, Jan. 2008.
- [20] J. R. Lamarsh and A. J. Baratta, *Introduction to Nuclear Engineering*. Pearson, 3rd ed., Mar. 2001.
- [21] D. L. Williams, “High Intensity, Pulsed, D-D Neutron Generator,” *Lawrence Berkeley National Laboratory*, Apr. 2010.
- [22] IAEA, “Neutron generators for analytic purpose,” *IAEA Radiation Technology Reports*, no. 1, 2012.
- [23] S. Chu, L. Ekstrom, and R. Firestone, *The Lund-LBNL Nuclear Data Search*. <http://nucleardata.nuclear.lu.se/toi/>, Accessed: June 2017.
- [24] S. Marsland, *Machine Learning: An Algorithmic Perspective, Second Edition*. CRC Press, Sept. 2015.
- [25] S. Ao, B. B. Rieger, and M. Amouzegar, *Machine Learning and Systems Engineering*. Springer Science & Business Media, Oct. 2010.
- [26] R. Brun and F. Rademakers, “Root - an object oriented data analysis framework,” *Nucl. Inst. & Meth. in Phys. Res.*, no. 389, 1997.
- [27] K. Gurney, *An Introduction to Neural Networks*. CRC Press, Aug. 1997.
- [28] M. F. Moller, “A scaled conjugate gradient algorithm for fast supervised learning,” *Neural Networks*, vol. 6, no. 4, pp. 525–533, 1993.
- [29] I. The MathWorks, “Matlab and statistics toolbox release,” no. 2016b, 2016.

- [30] S. Avdic, S. A. Pozzi, and V. Protopopescu, "Detector response unfolding using artificial neural networks," *Nuclear Instruments and Methods in Physics Research Section A: Accelerators, Spectrometers, Detectors and Associated Equipment*, vol. 565, pp. 742–752, Sept. 2006.
- [31] N. Ghal-Eh, P. Ahmadi, and V. Doost-Mohammadi, "A quantitative PGNAA study for use in aqueous solution measurements using AmBe neutron source and BGO scintillation detector," *Nuclear Instruments and Methods in Physics Research Section A: Accelerators, Spectrometers, Detectors and Associated Equipment*, vol. 808, pp. 123–127, Feb. 2016.
- [32] A. I. Skrypnyk, "Artificial neural networks in gamma spectrum based radionuclide identification," *Telecommunications and Radio Engineering*, vol. 75, no. 12, 2016.
- [33] R. E. Abdel-Aal and M. N. Al-Haddad, "Determination of radioisotopes in gamma-ray spectroscopy using abductive machine learning," *Nuclear Instruments and Methods in Physics Research Section A: Accelerators, Spectrometers, Detectors and Associated Equipment*, vol. 391, pp. 275–288, June 1997.
- [34] V. Doostmohammadi, D. Sardari, and A. M. Nasrabadi, "Combined application of Monte Carlo method and neural networks to simulate qualitative prompt gamma neutron activation analysis," *Journal of Radioanalytical and Nuclear Chemistry*, vol. 283, pp. 403–407, Dec. 2009.
- [35] F. J. O. Ferreira, V. R. Crispim, and A. X. Silva, "Detection of drugs and explosives using neutron computerized tomography and artificial intelligence techniques," *Applied Radiation and Isotopes*, vol. 68, pp. 1012–1017, June 2010.
- [36] W. V. Nunes, A. X. da Silva, V. R. Crispim, and R. Schirru, "Explosives detection using prompt-gamma neutron activation and neural networks," *Applied Radiation and Isotopes*, vol. 56, pp. 937–943, June 2002.

- [37] V. Vigneron, J. Morel, M. C. Lepy, and J. M. Martinez, "Statistical modelling of neural networks in $\hat{\text{I}}\text{s}$ -spectrometry," *Nuclear Instruments and Methods in Physics Research Section A: Accelerators, Spectrometers, Detectors and Associated Equipment*, vol. 369, pp. 642–647, Feb. 1996.
- [38] A. Varley, A. Tyler, L. Smith, and P. Dale, "Development of a neural network approach to characterise ^{226}Ra contamination at legacy sites using gamma-ray spectra taken from boreholes," *Journal of Environmental Radioactivity*, vol. 140, pp. 130–140, Feb. 2015.
- [39] M. Me and A.-H. A, "Application of Artificial Intelligence Methods in Quantitative Analysis of Gamma-ray Spectra," *Journal of Applied & Computational Mathematics*, pp. 1–3, Sept. 2015.
- [40] K. Peng, J. Yang, X. Tuo, H. Du, and R. Zhang, "Research on PGNAA adaptive analysis method with BP neural network," *Modern Physics Letters B*, vol. 30, p. 1650386, Nov. 2016.
- [41] S. Dragovic, A. Onjia, S. Stankovic, I. Anicin, and G. Bacic, "Artificial neural network modelling of uncertainty in gamma-ray spectrometry," *Nuclear Instruments and Methods in Physics Research Section A: Accelerators, Spectrometers, Detectors and Associated Equipment*, vol. 540, pp. 455–463, Mar. 2005.
- [42] J. Damgov and L. Litov, "Application of neural networks for energy reconstruction," *Nuclear Instruments and Methods in Physics Research Section A: Accelerators, Spectrometers, Detectors and Associated Equipment*, vol. 482, pp. 776–788, Apr. 2002.
- [43] S. Sharma, C. Bellinger, N. Japkowicz, R. Berg, and K. Ungar, "Anomaly detection in gamma ray spectra: A machine learning perspective," in *2012 IEEE Symposium on Computational Intelligence for Security and Defence Applications*, pp. 1–8, July 2012.

- [44] M. R. Kardan, R. Koochi-Fayegh, S. Setayeshi, and M. Ghiassi-Nejad, "Fast neutron spectra determination by threshold activation detectors using neural networks," *Radiation Measurements*, vol. 38, pp. 185–191, Apr. 2004.
- [45] P. E. Keller and R. T. Kouzes, "Gamma spectral analysis via neural networks," in *Nuclear Science Symposium and Medical Imaging Conference, 1994., 1994 IEEE Conference Record*, vol. 1, pp. 341–345 vol.1, Oct. 1994.
- [46] E. E. Zadeh, S. A. H. Fegghi, G. H. Roshani, and A. Rezaei, "Application of artificial neural network in precise prediction of cement elements percentages based on the neutron activation analysis," *The European Physical Journal Plus*, vol. 131, p. 167, May 2016.
- [47] S. Akkoyun, T. Bayram, and S. O. Kara, "Improvement studies on neutron-gamma separation in hpge detectors using neural networks," *Cumhuriyet Science Journal*, vol. 34, no. 1, pp. 42–51, 2013.
- [48] H. Sang, F. Wang, L. Liu, and H. Sang, "Detection of element content in coal by pulsed neutron method based on an optimized back-propagation neural network," *Nuclear Instruments and Methods in Physics Research Section B: Beam Interactions with Materials and Atoms*, vol. 239, pp. 202–208, Sept. 2005.
- [49] T. Goorley, M. James, T. Booth, F. Brown, J. Bull, L. J. Cox, J. Durkee, J. Elson, M. Fensin, R. A. Forster, J. Hendricks, H. G. Hughes, R. Johns, B. Kiedrowski, R. Martz, S. Mashnik, G. McKinney, D. Pelowitz, R. Prael, J. Sweezy, L. Waters, T. Wilcox, and T. Zukaitis, "Initial mcnp6 release overview," *Nuclear Technology*, vol. 180, no. 3, pp. 298–315, 2012.
- [50] J. W. Durkee, M. R. James, G. W. McKinney, L. S. Waters, and T. Goorley, "The MCNP6 Delayed-Particle Feature," vol. 180, no. 3, pp. 336–354, 2012.

- [51] A. Azbouche, M. Belgaid, and H. Mazrou, “Monte Carlo calculations of the HPGe detector efficiency for radioactivity measurement of large volume environmental samples,” *Journal of Environmental Radioactivity*, vol. 146, pp. 119–124, Aug. 2015.
- [52] K. Fantinova and P. Fojtik, “Monte Carlo simulation of the BEGe detector response function for in vivo measurements of ^{241}Am in the skull,” *Radiation Physics and Chemistry*, vol. 104, pp. 345–350, Nov. 2014.
- [53] W. B. Wilson, S. Cowell, T. R. England, A. C. Hayes, and P. Moller, “A Manual for CINDER’90 Version 07.4 Codes and Data,” no. LA-UR-07-8412, 2007.

VITA

Huseyin Sahiner received a PhD degree in July 2017 from Nuclear Engineering at Missouri University of Science and Technology. He worked with Xin Liu, Dr. on neutron activation analysis techniques. He received his BS degree in physics from Cukurova University of Turkey. He had been awarded by TUBITAK-BAYG (Scientific and Research Council of Turkey-Young Scientist Support Group) during his BS degree. He received his MS degree in particle physics also from Cukurova University with a partial work from Aristotle University of Thessaloniki of Greece. He was selected to be supported by Erasmus student exchange program for this partial work. His MS work was to analyze muon drift chamber's performance for ATLAS at Cern. He also received an MA degree in teaching excellence in physics from Cukurova University. Afterwards, he started his PhD in Mechanical Engineering in South Carolina before changing the subject to Nuclear Engineering. He was selected by Turkish Government to be supported for a science degree abroad. His interest was on radiation detection and measurement, neural network, Monte Carlo simulation.